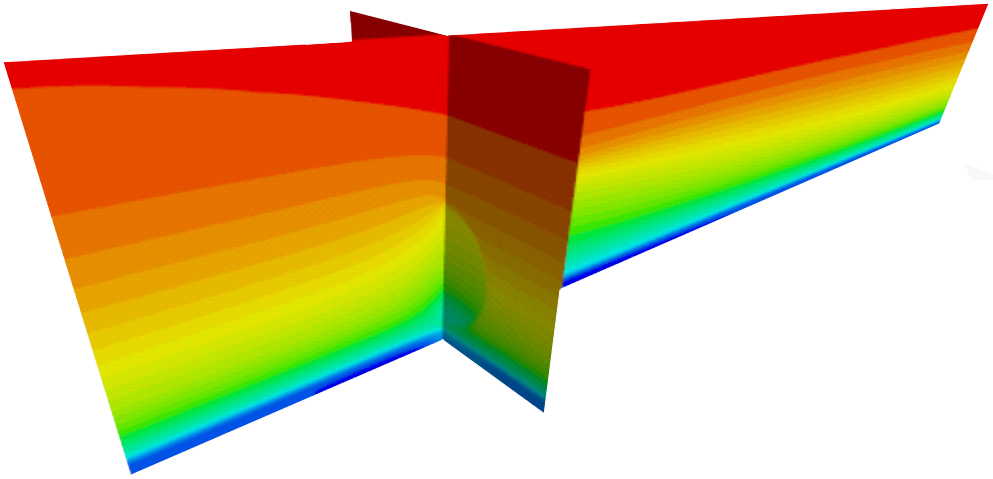

CFD Modelling of the Neutral Atmospheric Boundary layer above and inside Forest Regions

Bachelor's thesis in Mechanical Engineering

Viktor Alatalo
Tim Johansson
Viktor Larsson
Sara Eriksson
Oscar Larsson

DEPARTMENT OF MECHANICS AND MARITIME SCIENCES

CHALMERS UNIVERSITY OF TECHNOLOGY
Gothenburg, Sweden 2020
www.chalmers.se

BACHELOR THESIS 2020:10

CFD Modelling of the Neutral Atmospheric Boundary layer above and inside Forest Regions

Bachelor thesis in Mechanics and Maritime Sciences

Viktor Alatalo | Sara Eriksson | Tim Johansson
Oscar Larsson | Viktor Larsson

CHALMERS
UNIVERSITY OF TECHNOLOGY

Department of Mechanics and Maritime Sciences
Division of Fluid Dynamics
CHALMERS UNIVERSITY OF TECHNOLOGY
Gothenburg, Sweden 2020

CFD Modelling of the Neutral Atmospheric Boundary layer
above and inside Forest Regions

VIKTOR ALATALO, SARA ERIKSSON, TIM JOHANSSON, OSCAR LARSSON
and VIKTOR LARSSON

Supervisor: Dr. Hamidreza Abedi, Division of Fluid Dynamics
Examiner: Prof. Lars Davidson, Division of Fluid Dynamics

Bachelor Thesis 2020:10
Department of Mechanics and Maritime Sciences
Chalmers University of Technology
SE-412 96 Gothenburg
Sweden
Telephone: +46 (0)31-772 1000

Cover: Wind visualization constructed in STAR-CCM+ showing the airflow around a wind turbine and forest canopy.

Printed by Department of Mechanics and Maritime Sciences
Gothenburg, Sweden 2020

Abstract

As the demand for wind power increases, more areas are being investigated for construction of wind farms. The forest covered landscape of Sweden offers plenty of room for expansion, but comes with certain difficulties. One important factor to consider is that the forest canopies are sources of turbulence in the air flow. The turbulence causes fatigue in wind turbines and may affect their power production, it therefore needs to be taken into account when constructing them. One cost-effective method for recreating and measuring the effects of this turbulence is Computational Fluid Dynamics (CFD). In this project, the commercial software STAR-CCM+ was used for all simulations. Using CFD, the turbulence may be modelled in several different ways. Large-Eddy Simulations (LES) is a turbulence model that accurately predicts turbulent, unsteady flow, but at the cost of computational power. Another model uses the Reynolds-Averaged Navier-Stokes equations (RANS) which solve for the mean velocity field by modelling the fluctuations in the flow. LES was used for reference data, but the main part of the project was performed using RANS in combination with the k-ϵ model. Several different simulations were performed aiming to replicate the real physical conditions. In addition to bare terrain, two different forests were simulated, 'sparse' and 'dense'. This project employed four canopy models: Sanz, Svensson, Green and Liu. Of these models, Sanz was found to correspond best with the LES data. After choosing a canopy model, a wind turbine was simulated by employing the 'virtual disk' model available in STAR-CCM+. The forest density was found to have little impact on the streamwise velocity of the wind. The turbulent kinetic energy, however, differed with the forest density. For the wind turbine simulations the same relation was observed, as the turbulent kinetic energy was higher when the forest was included compared to bare terrain. This increase bears significance on the lifespan of wind turbines, and by extension, their design. Testing a wider range of wind speeds, as well as investigating whether wake regions yield similar effects may be topics for future studies.

Keywords: Wind power production, Turbulence modelling, RANS, LES, k-epsilon, STAR-CCM+, Actuator disc, Canopy models, Neutral ABL

Acknowledgements

We would like to thank Dr. Hamidreza Abedi for all the guidance and knowledge he has provided during the course of this project. His expertise in fluid mechanics and STAR-CCM+ has been essential to the progress and results of the project. We would also like to thank Chalmers Centre for Computational Science and Engineering for providing resources for our simulations.

Viktor Alatalo, Sara Eriksson, Tim Johansson, Oscar Larsson and Viktor Larsson,
Gothenburg, May 2020

Nomenclature

Abbreviations

ABL Atmospheric Boundary Layer

CFD Computational Fluid Dynamics

DNS Direct Numerical Simulation

FVM Finite Volume Method

LAD Leaf Area Density

LAI Leaf Area Index

LES Large Eddy Simulation

NREL National Renewable Energy Laboratory

PAD Plant Area Density

RANS Reynolds Averaged Navier-Stokes

RMSE Root Mean Square Error

TDR Turbulent Dissipation Rate

TI Turbulence Intensity

TKE Turbulent Kinetic Energy

List of Symbols

$\bar{(.)}$ Time averaged quantity

$\bar{v}_{1,hub}$ Mean streamwise velocity component at hub height

$\bar{v}_{1,ref}$	Reference wind speed
β_d	Canopy model constant
β_p	Canopy model constant
ϵ	Turbulent dissipation rate
$\mathbf{v}$	Flow velocity vector
ν_t	Turbulent kinematic viscosity
σ_ϵ	$k-\epsilon$ model constant
σ_k	$k-\epsilon$ model constant
a_f	Leaf area density
C_μ	$k-\epsilon$ model constant
C_d	Forest drag coefficient
C_y	Effective drag coefficient
$C_{\epsilon 1}$	$k-\epsilon$ model constant
$C_{\epsilon 2}$	$k-\epsilon$ model constant
$C_{\epsilon 4}$	Canopy model constant
$C_{\epsilon 5}$	Canopy model constant
h	Tree height
k	Turbulent kinetic energy
p	Pressure
Re	Reynolds number
Re_{crit}	Critical Reynolds number
S_ϵ	Turbulent dissipation sink & source term
S_k	Turbulent kinetic energy sink & source term
S_u	Momentum sink term

S_{ij}	Deformation tensor component
u_τ	Wall friction velocity
U_b	Bulk velocity
v_i	i:th flow velocity component
x, y, z	Streamwise, vertical and spanwise direction
y_{hub}	Hub height of wind turbine
y_{ref}	Reference height
y_0	Surface roughness length

Contents

1

Introduction

During recent years the demand for sustainable power sources has grown, leading to an increase in research especially for wind energy as a renewable source of electricity. Since Sweden introduced a policy for net zero emissions by 2045 [1], the interest in substantially expanding wind power production has risen. From 2004 to 2018 the proportion of energy production from wind power in Sweden increased from 1% to 10.4% [2]. This expansion has led to the most suitable locations for wind power farms being occupied. Thereby there is presently an emerging need for alternative locations to further expand wind power farms. The proportion of forested land area in Sweden is around 70% [3]. Because of this, new technical and environmental issues must be addressed. One such issue is how the expansion of wind power farms in forest regions would affect the efficiency of wind turbines. In a candidate wind farm area it is preferable to experimentally measure the wind. Before wind farms are installed, on-site measurements are performed to show wind patterns in that area. In practice this is expensive and takes a couple of years to perform. Therefore, numerical simulations are used as an alternative to on-site measurements.

Areas occupied by wind parks today usually lack disturbances such as trees and hills. If turbulence caused by forest canopies leads to a higher fatigue load or lower power production in wind turbines, investors might not prefer to invest in such wind farms. Hence, Computational Fluid Dynamics (CFD) can be used to model the wind field to estimate the annual power production. In addition CFD can be used to evaluate turbulence in order to avoid locations which might lead to a higher fatigue load. Looking at the areas above and inside forest regions, the wind patterns are not easy to simulate. Because of the difficulty in predicting these patterns there is a greater need for more accurate modelling, but with an increased need for higher accuracy the computational cost increases drastically. A good numerical wind resource prediction can be used as an effective tool for expanding the number of wind farm parks which assists in locating the most suitable locations for maximising power production and minimising fatigue loads.

1.1 Purpose

The purpose of this Bachelor's thesis is to simulate the airflow over and inside homogeneous forest regions to find out how forest canopies affect mean power production of wind farms. One part of the project will be looking into the modelling of the forest which is supposed to have a great impact on the mean velocity profile. Continued analysis using different leaf area density profiles will be performed to determine how different types of forest will affect the generated mean power.

In order to complete the simulations within the limitations of the project, RANS turbulence modelling will be used to perform the simulations faster. The analysis concerning turbulence modelling will be dedicated towards determining if RANS turbulence modelling is accurate enough in this study. This will be done by comparing results to a provided LES which is a more accurate model.

For this purpose four different canopy models will be analysed and the one most suited for this project will be used for further simulations concerning different wind speeds etc. Different wind speeds are simulated in order to draw conclusions about whether a forest will affect winds near a wind turbine in such a way that the rated speed with maximum power production is attainable. In addition, the different wind speed simulations will also allow analysis for whether the chosen model is accurate for all wind speeds.

1.2 Limitations

This bachelor's thesis will be limited to modelling the airflow under the neutral atmospheric condition using the commercial software, STAR-CCM+. The simulations done in the CFD software are limited by the computational resources available to the group. For the simulations the Reynolds-Averaged Navier-Stokes turbulence model will be used. The simulations will be done in a horizontally homogeneous forest. Complex terrain such as hills, open water and clearings will not be included in the computational domain.

The study will only cover steady flow. As for other attributes of the simulated forest, the simulations will be run with different settings for forest density. Two different forest densities and simulations without any forest will be performed. Four wind speeds will be studied in order to compare their impacts on mean energy production. The wind speeds are 5, 8, 12 and 20 m/s.

The simulations that are run with a wind turbine use a simplified model where a disk will be used in place of the complex geometry of a rotor and blades. The tower of the turbine will not be included in the computational domain. Only a single wind turbine will be simulated and wake effects on other turbines will therefore not be part of this study. To make investigation of the movement of fluids simpler, small-scale flow structures where separate atoms may have an effect are ignored.

1.3 Outline of the thesis

This report consists of 5 chapters: introduction, theory, method, result and conclusions. Chapter two contains general theory about fluid mechanics, wind power production and CFD. In chapter three the method used in this bachelor's thesis is described. In chapter four the results are shown with tables and figures along with relevant discussion. In the last chapter conclusions are drawn regarding the results and the purpose of the project.

2

Theory

A fluid flowing through space is affected by forces and behaves differently depending on the conditions of that particular space. When observing how the wind moves, it seems random. The fundamental reason behind its movement can be found in the theory of fluid mechanics which will be explained in the following chapter. To simplify the simulation of the wind, different assumptions and models will be used, explained further in this chapter.

2.1 Fluid Mechanics

When a fluid is in contact with a solid surface the fluid velocity component normal to the solid surface is zero. This can be understood by considering a river. The water can not flow though large rocks and must go around them. Assuming the water is approaching the rocks, the water's velocity component normal to the rocks' surface must eventually become zero. At the surface of the rock, the approaching water comes to a complete stop which pushes all surrounding water to the sides, tangent to the surface. In all cases when a fluid in motion approaches a surface the fluid comes to a complete stop and assumes a zero velocity relative to the surface. This is because the fluid sticks to the surface due to viscous effects. This is known as the no-slip condition. Due to the no-slip condition a logarithmic velocity profile will develop, see Fig. 2.1. Closer to the surface the viscous effects are significant and the velocity gradient becomes higher. The region where the surrounding flow is affected by a surface is called the boundary layer.

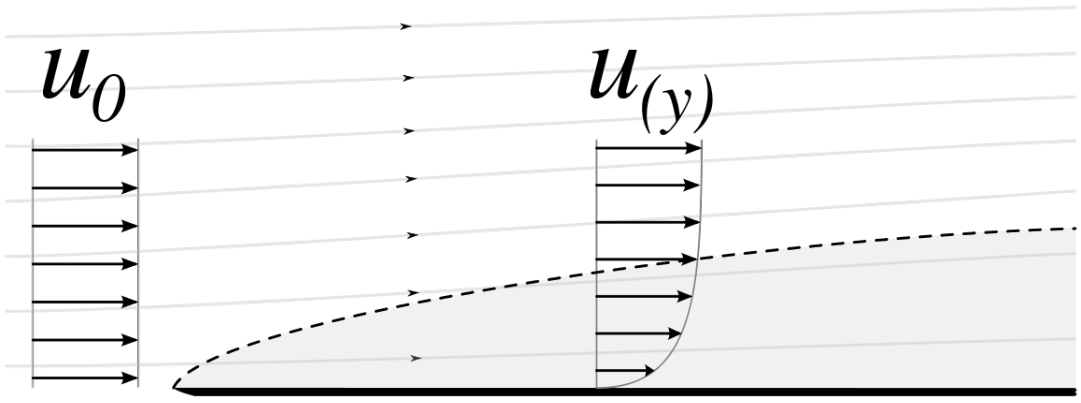

Figure 2.1: Developing velocity profile, inside of the wall boundary layer. [4]

Flow that does not change temporally is called steady state flow. This means that at any point the properties of the fluid remain constant, but can differ from point to point. In incompressible flow the density is approximated to be constant throughout the flow when the pressure changes, this also means the volume of the fluid remains unchanged. When changes in density are very small the governing equations of fluid motion are greatly simplified. One other property that can help simplify solving is if the flow is laminar. Fluid flow can be divided into two main categories, laminar and turbulent. Which of the two is present is determined by the Reynolds number and the surrounding geometry, for example pipe or flat plate flow. These two types of flow will be described in detail in section 2.3.

Finally viscosity is the fluid's resistance to motion. Viscosity can be compared to friction that emerges between two solid bodies. When a fluid moves near a solid or if two different fluids move next to each other the viscosity affects the flow. Viscosity is the fluid's resistance to motion by itself. It can therefore be described as the measure of a fluid's resistance to shear or deform. Viscosity is usually expressed by dynamic viscosity, μ and the unit is kg/m·s or N·s/m^2. The kinematic viscosity, ν, is the ratio of dynamic viscosity to density $\nu = \mu/\rho$.

2.2 Wind Power Production

There are three main factors that influence power output: wind speed, air density, and the rotor radius of the turbine. Wind speed largely determines the amount of energy which can be extracted by a turbine. Higher speeds generate more power since stronger winds allow the blades to capture more kinetic energy, which in turn translates to more electrical power from the generator. The air density and rotor radius directly affect the air volume that passes through the turbine, and therefore also the power output.

Wind power is proportional to the cube of the mean wind speed. This proportionality is derived from the definition of kinetic energy, given by

$$E = \frac{1}{2}mv^2 = \frac{1}{2}\rho V v^2 \tag{2.1}$$

where ρ, V and v denote air density, air volume and wind speed, respectively. Since the air flow rate is equal to the mean wind speed times the area it passes through, Eq. 2.2 may be used, where A and t denote the rotor area and time, respectively. This equation shows the importance of wind speed to the power production of a turbine. As the wind speed doubles, the produced power increases by a factor of eight in an ideal case. The power production is also affected by the local air density, which is a function of altitude, as well as the pressure and temperature of the air.

$$P = \frac{E}{t} = \frac{1}{2}\rho V v^2 = \frac{1}{2}A\rho v^3 \tag{2.2}$$

Wind turbines are designed to operate within a specific range of wind speeds. The limits of the range are known as the cut-in speed and cut-out speed. The cut-in speed is the point where the wind turbine is able to generate power, while the cut-out speed is when the turbine must be shut down to avoid damage. Between these limits lie the rated speed, where the turbine is able to generate power at its maximum capacity. The relation between wind speed and power output is illustrated in Fig. 2.2.

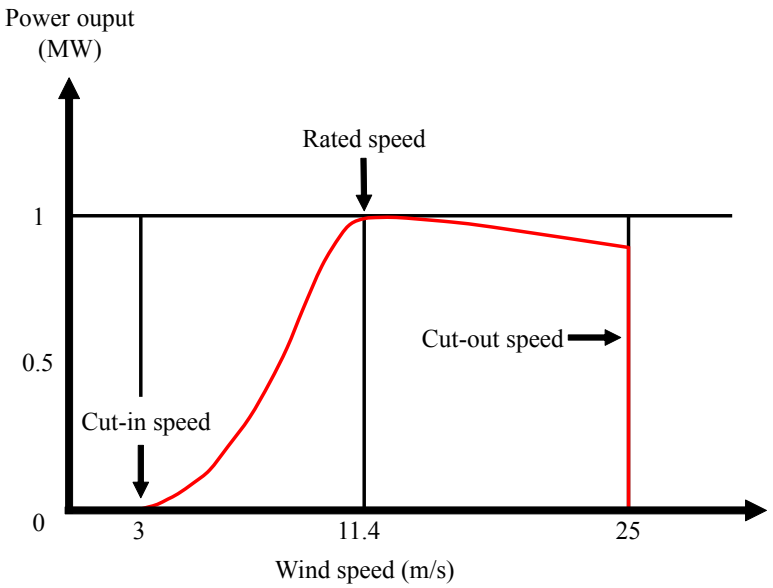

Figure 2.2: Example power curve for 5-MW wind turbine.

In order to control the power production of the wind turbine when the wind speed is above the rated speed of the turbine, blade pitch regulation must be used. This means increasing the blades' angle of attack. Doing this makes it possible for more wind to pass by the turbine blades which keeps power production almost constant with increasing wind speeds. Above the cut out speed further blade pitch regulation is unsafe, the wind is too strong and the blades are stopped. To keep the rotor facing into the wind as the wind direction changes, the yaw drive allows the entire turbine nacelle to rotate to face the wind. This is required to be able to capture the wind with maximum efficiency. If the turbine nacelle could not rotate, the yaw of the wind would affect fatigue load and power output.

Wind turbines are often grouped together in so-called wind farms. The placement of the turbines in relation to each other will affect their power output, due to wake effects. Downstream from a turbine rotor, an aerodynamic wake region is created, which results in reduced wind speed and increased turbulence. These effects have to be taken into consideration when constructing a wind farm. In addition to the wake effects, turbulence as a result of forest or complex terrain has to be accounted for. The additional turbulence due to forest canopies is studied in this thesis. Underestimating these effects can lead to under-dimensioned turbines which results in significantly shortened lifespans.

2.2.1 Reference wind turbine

When decisions are made for this project they are taken in reference to a real wind turbine. The one chosen to look at was the 5-MW National Renewable Energy Laboratory reference wind turbine and many of the decisions are based on the operating conditions and size of this wind turbine. The most valuable statistics are presented in Tab. 2.1. The hub height and rotor blade radius are displayed in Fig. 2.3.

Table 2.1: 5-MW NREL Reference Wind turbine [5].

Property	Values
Rating	5 MW
Cut-In Wind Speed	3 m/s
Rated Wind Speed	11.4 m/s
Cut-Out Wind Speed	25 m/s
Cut-In Rotor speed	6.9 rpm
Rated Rotor Speed	12.1 rpm
Rotor Diameter	126 m
Hub Diameter	3 m
Hub Height	90 m

Looking at the cut in- and cut-out wind speed, it was decided to simulate wind speeds within that interval to be able to evaluate the power output. To investigate wind speeds below or above the interval would be unnecessary since the wind turbine would not produce any power outside this interval. The size of the wind turbine will be used when designing the simulation domain and when deciding certain boundary conditions which will be further explained in chapter 3.

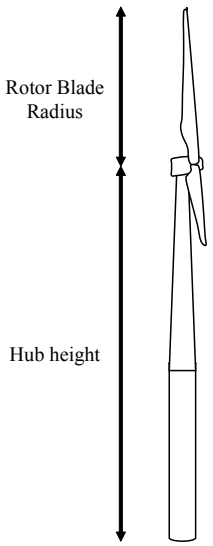

Figure 2.3: Wind turbine 5 MW

2.3 Turbulence

Fluid flow can be divided into two main categories, turbulent and laminar. The characteristics of laminar flow is steady, smooth flow without fluctuations or significant mixing. Laminar flow usually occurs at low flow rates, but is ultimately determined by the Reynolds number, see Eq. 2.3. The critical Reynolds number Re_{crit} is a specific Reynolds number and it is defined as laminar flow transitioning into turbulent flow. It is dependent on the geometry such as pipe flow with Re_{crit} 2300 - 4000, or flow over a flat plate with Re_{crit} 10^5 - 10^6 [6].

$$Re = \frac{\rho V D}{\mu} \tag{2.3}$$

where ρ, V, D and μ denote the density of the fluid, the velocity of the fluid, the characteristic linear dimension or relative scale and the dynamic viscosity, respectively.

The opposite of laminar flow is called a turbulent flow which occurs at higher velocities. Turbulence is not well defined, but it has certain characteristics such as being diffusive, dissipative, three dimensional, chaotic and occurring at Reynolds numbers above the critical Reynolds number. Most naturally occurring flows are turbulent with notable examples such as the wind and even subtle air movements in a still room.

In turbulent flow there are rotational structures called eddies that come in different sizes, or scales. The larger ones extract kinetic energy from the mean flow, and through a cascading process transfer that energy to progressively smaller eddies [7]. At the smallest scales, the energy is dissipated rapidly through viscous stresses, and converted to thermal energy. The large eddies behave differently depending on direction, while the smaller ones do not (they are anisotropic and isotropic, respectively).

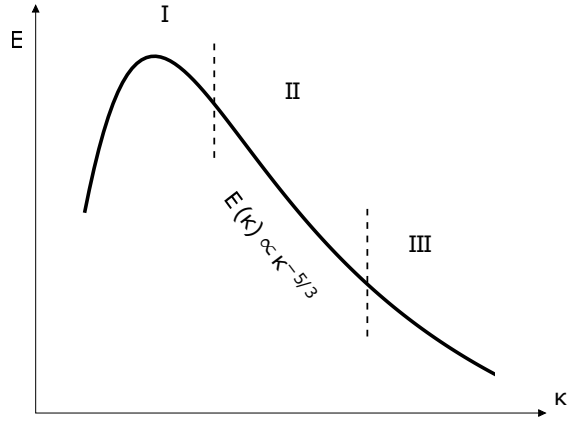

Figure 2.4: The energy spectrum marked with the three different regions [7]. The large eddies in region I hold most of the energy. In a cascading process, energy is transported through region II and finally dissipated in region III by the small eddies.

The turbulent fluctuations (of the flow velocity) can be treated in wavenumber space by describing them with a Fourier series [7]. An eddy can thus be assigned a wavenumber (κ) which is proportional to the inverse of its length scale. Each eddy carries energy, $E(\kappa)$, i.e. energy in wavenumber space. The turbulent eddies come in a wide range of scales, therefore there is a spectrum of energy, as illustrated by Fig. 2.4. The kinetic energy of the turbulence is the area under the graph. The spectrum can be divided into three regions. Region I contains the large eddies which hold most of the energy and interact with the mean flow. Region II contains the smallest and dissipative eddies. The intermediate region II, holds those eddies which are too large to convert energy to heat, but small enough for their behaviour to be governed by the rate at which the smallest eddies dissipate energy [8]. The Kolmogorov spectrum law predicts the spectral energy to decay within the intermediate region as

$$E \propto \kappa^{-5/3} \tag{2.4}$$

2.4 CFD

Laminar flow can generally be solved analytically however turbulent flow must be solved mainly by numerical simulations. Therefore Computational Fluid Dynamics (CFD) is used to solve the equations numerically. CFD is the analysis of fluid flows using numerical solution methods. These methods use different techniques, finite difference, finite element and spectral methods. In this project the Finite Volume Method (FVM) is used. FVM is a special finite difference formalisation space [9]. The model utilizes the Navier-Stokes equations. The domain is divided into a large number of control volumes. The equations are solved for every control volume, also called cell. These cells make a volume mesh. More cells in the mesh give a better approximation but also increase the computational time.

Some of the advantages with CFD beside the ability to model airflow is the reduction in lead time and cost of the experiments and investigations. The detail of results is also practically unlimited, but this will cost in time and capacity. Another advantage with CFD is the ability to study systems which are difficult to construct or systems under hazardous conditions [8].

Fluent, COMSOL and STAR-CCM+ are some of the most common commercial software that are used for CFD-simulations. In this project STAR-CCM+ will be used. The reason for using STAR-CCM+ is that it is a user-friendly software and is the CFD software used at Chalmers. STAR-CCM+ is available for both Linux and Windows. Objects created in the most popular 3D modelling programs can easily be imported and used in simulations in STAR-CCM+. It is easy to make changes and setups for the simulations do not need to be repeated when replacing parts or performing other modifications.

To perform any CFD simulation, the geometry, fluid properties, boundary conditions and mesh must be properly specified. In addition, depending on the problem, an appropriate solver must be chosen. In this work the k-ϵ RANS turbulence model will be used, explained further in section 2.5.2.

2.4.1 Boundary Conditions

The area studied is a flat ground without any irregularities such as non-repeating large hills or heterogeneous forest canopies. This enables the use of periodic boundaries in the simulations, which means that the flow at the outlet is directly and continuously fed back

to the inlet. This lets the flow more quickly develop completely. When using periodic boundaries only a mass flux is given as starting condition, for example in kilogram per second. This starts out as a plane of mass flow at the inlet, but quickly develops into a familiar velocity curve as the simulation progresses, see Fig. 2.1. Since the outlet is continuously fed to the inlet, a proper velocity profile will be developed in the entire simulated volume when the flow is fully-developed. Mathematically, the periodic boundary condition can be written as

$$\psi(x + L_x, y, z) = \psi(x, y, z) \tag{2.5}$$

$$\psi(x, y, z + L_z) = \psi(x, y, z) \tag{2.6}$$

where L_x and L_z denote the domain length in the streamwise direction and in the spanwise direction, respectively. Note that for this project, only the inlet, outlet and side boundary conditions are periodic.

Apart from periodic boundary conditions, when an inlet-outlet boundary is used in a simulation, an inlet velocity profile for the airflow must be explicitly given. The length of the computational domain also needs to be longer to be able to evaluate the effects of flow structures such as wakes. This is because the flow only passes though the domain once and therefore needs space to become fully-developed. The advantages with this technique is that is can be used when there are irregularities in the domain.

A wall boundary doesn't allow any fluid to pass through it and uses the no slip condition, it also has a certain roughness. A symmetric boundary condition makes it possible to see the lower part of the atmosphere as the lower half of a giant channel flow and therefore the height can be reduced. Any airflow that would cross the symmetric boundary will instead be reflected, this becomes a problem if such currents were to significantly influence the flow close to the ground.

2.4.2 Modelling the wind turbine

When energy is extracted from the wind, a wake is created where the turbulence intensity is increased and the mean wind velocity is decreased. Usually in wind farms, most of the turbines operate in the wake of other turbines. This placement reduces the power production. To simulate the wake of the wind turbine, the actuator disc model is used. This is one of the most common methods. It is practical when effects on surroundings are desired while the behaviour of the rotor is available. In this model the rotor is assumed to be an actuator disc, with no blade details. The forces from the rotor blades are equally distributed on the circular disc. The main benefit with the actuator

disc is that the viscous airfoil boundary layer is not resolved. This makes the study of the wake easier.

The area of the disc is smaller than the cross-sectional area of its wake downstream. The upstream cross-sectional area of the same flow volume is smaller than the disc area, see Fig. 2.5. The mass flow is equal at every cross-section. For each cross-section the mass flow can be calculated by Eq. 2.7.

$$\dot{m} = (\rho AU)_0 = (\rho AU)_D = (\rho AU)_3 \tag{2.7}$$

where ρ, A and U denote the density of the air, the cross-section area and the mean streamwise velocity, respectively.

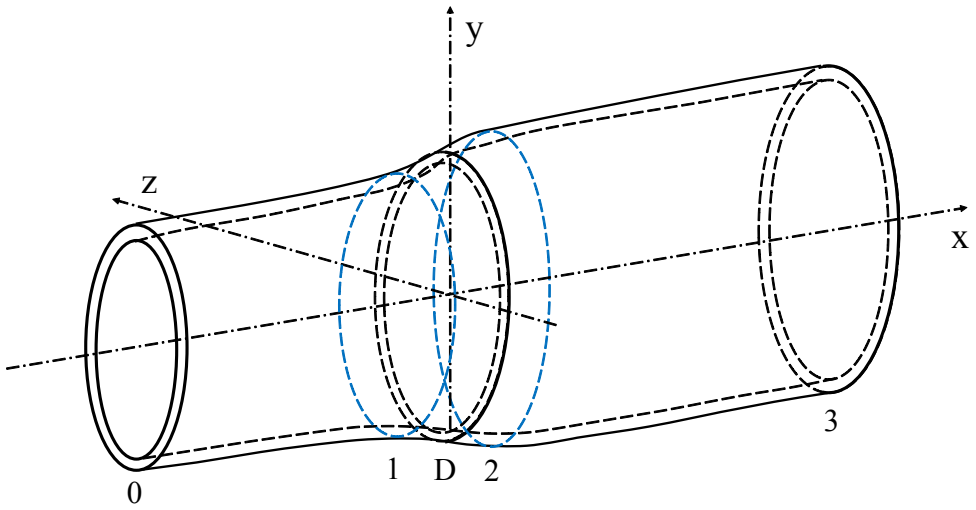

Figure 2.5: Actuator disc model, D is the disc, surrounding points of interest are labeled from upstream starting at point 0.

In STAR-CCM+ the actuator disc model is called 'virtual disk'. The one-dimensional momentum theory is the simplest way to express the actuator disc. The actuator disc is modelled as a source term in the momentum equation. The actuator disc model is based on Bernoulli's equation, see Eq. 2.8 [10]. In the equation, the streamwise flow velocity is the same before and after the disc. Likewise the pressure before the disc is the same as the pressure behind it. In other words the pressure $p_0 = p_3$ with points seen in Fig. 2.5.

With these assumptions an expression for the wind turbine thrust, T, and power

extraction, P, can be found, see Eqs. 2.9 and 2.10.

$$\frac{p_2 - p_1}{\rho} + \frac{1}{2}(U_2^2 - U_1^2) + g(h_2 - h_1) = 0 \tag{2.8}$$

where p, ρ, U, g and h denote the pressure, the density of the air, the velocity, acceleration due to gravity, and the length from the reference height, respectively.

$$T = \frac{1}{2}\rho A_D U_0^2 4a(1-a) \tag{2.9}$$

$$P = \frac{1}{2}\rho A_D U_0^3 4a(1-a)^2 \tag{2.10}$$

where A and a denote the cross-section area and the axial interference factor, respectively. The axial interference factor is defined as $a = 1 - \frac{U_D}{U_0}$.

2.5 Turbulence models

To be able to predict the wind flow well, models are needed. This is because models use approximations which make the process cheaper in terms of computational time. RANS turbulence models predict mean flow, which helps in reducing computational cost. Large-Eddy Simulation (LES) works with unsteady flow and predicts the instantaneous flow field. The result of this is that LES is generally more accurate in predicting flow, especially highly turbulent flow such as the wake behind a wind turbine. The following models are used in this project to create the simulations of the wind flow.

2.5.1 Reynolds-Averaged Navier-Stokes equations

The governing equations of the flow are the three Navier-Stokes equations together with the continuity equation, which express the conservation of momentum and conservation of mass, respectively. Solving these equations yields the flow field. However, a direct numerical simulation (DNS) is extremely costly in terms of computational resources. For the purposes of this project, solving the mean velocity field is sufficient.

The 'Reynolds decomposition' is the separation of instantaneous physical quantities into two parts, $\phi = \bar{\phi} + \phi'$. The bar indicates the mean and the prime denotes fluctuations or deviations from the mean. Using the decomposition, the governing equations can

be expressed as time averaged equations. For a steady and incompressible flow the Reynolds-Averaged Navier-Stokes (RANS) can be read

$$\frac{\partial(\bar{v}_j\bar{v}_i)}{\partial x_j} = -\frac{1}{\rho}\frac{\partial \bar{p}}{\partial x_i} + \frac{\partial}{\partial x_j}\left(\nu\frac{\partial \bar{v}_i}{\partial x_j} - \overline{v_j' v_i'}\right) \tag{2.11}$$

$$\frac{\partial \bar{v}_i}{\partial x_i} = 0 \tag{2.12}$$

The left side of the Eq. 2.11 represents the change in momentum due to convection. The first term on the right side, $\partial\bar{p}/\partial x_i$, is the mean pressure gradient acting on the fluid. The second term describes the diffusion, which includes the Reynolds stresses, $\overline{v_j' v_i'}$, due to turbulence. Equation 2.12 is the continuity equation.

The Reynolds stress tensor introduces six time-dependent variables which (in the RANS model) are modelled rather than solved for. The stresses are assumed to depend on the deformation caused by the mean flow $\bar{S_{ij}}$, and they are approximated by the 'Boussinesq assumption' as

$$-\overline{v_i' v_j'} = 2\nu_t \bar{S_{ij}} - \frac{1}{3}\delta_{ij}\overline{v_k' v_k'} = \nu_t\left(\frac{\partial \bar{v}_i}{\partial x_j} + \frac{\partial \bar{v}_j}{\partial x_i}\right) - \frac{2}{3}\delta_{ij}k \tag{2.13}$$

where ν_t, δ_{ij} and k denote the turbulent eddy viscosity, the Kronecker delta and the turbulent kinetic energy (TKE), respectively. The turbulent viscosity is a non-constant property of the flow (not the fluid). Depending on turbulence model, the definition of ν_t varies. In this project the k-ϵ turbulence model is used, in which ν_t is expressed as

$$\nu_t = C_\mu \frac{k^2}{\epsilon} \tag{2.14}$$

where C_μ and ϵ represent the k-ϵ model constant and the turbulent dissipation rate (TDR), respectively.

2.5.2 The k-ϵ model

The k-ϵ model is an eddy viscosity model. In the k-ϵ model two equations are used, these are called the k equation and the ϵ equation. These equations are used to calculate k and ϵ, respectively which are used to calculate the turbulent kinematic viscosity, see Eq. 2.14. The k and ϵ transport equations are used to determine the k equation and the ϵ equation. The transport equations are determined from the Navier-Stokes equations. The modelled k equation can be written as Eq. 2.15 [11].

$$\overline{v}_j \frac{\partial k}{\partial x_j} = \nu_t \left[\frac{\partial \overline{v}_i}{\partial x_j} + \frac{\partial \overline{v}_j}{\partial x_i} \right] \frac{\partial \overline{v}_i}{\partial x_j} + \frac{\partial}{\partial x_j} \left[\left(\nu + \frac{\nu_t}{\sigma_k} \right) \frac{\partial k}{\partial x_j} \right] - \epsilon \tag{2.15}$$

where ν, ν_t, k, σ_k and ϵ denote laminar kinematic viscosity, turbulent kinematic viscosity, turbulent kinetic energy, turbulent Prandtl number for k and dissipation, respectively. From the k equation the modelled ϵ equation can be derived.

$$\overline{v}_j \frac{\partial \epsilon}{\partial x_j} = \frac{\epsilon}{k} C_{\epsilon 1} \nu_t \left[\frac{\partial \overline{v}_i}{\partial x_j} + \frac{\partial \overline{v}_j}{\partial x_i} \right] \frac{\partial \overline{v}_i}{\partial x_j} + \frac{\partial}{\partial x_j} \left[\left(\nu + \frac{\nu_t}{\sigma_\epsilon} \right) \frac{\partial \epsilon}{\partial x_j} \right] - C_{\epsilon 2} \frac{\epsilon^2}{k} \tag{2.16}$$

where $C_{\epsilon 1}$, σ_ϵ and $C_{\epsilon 2}$ denote a constant, turbulent Prandtl number for ϵ and a constant, respectively.

To solve the equations for different cases some universal constants need to be determined, see section 2.7. C_μ from Eq. 2.14. σ_k in the k-equation, as well as $C_{\epsilon 1}$, $C_{\epsilon 2}$ and σ_ϵ in the ϵ equation. The constants used can be seen in Tab. 2.2

Table 2.2: Values used for the $k - \epsilon$ model constants.

Constant	C_μ	$C_{\epsilon 1}$	$C_{\epsilon 2}$	σ_k	σ_ϵ
Value	0.09	1.44	1.9	1.0	1.2

There are several different turbulence models that can be used to model flow. The advantage with the k-ϵ model is that it is simple to use, and it has been extensively used in many different applications. There are some disadvantages as well. This model is not good at predicting normal stresses. Despite the disadvantages, the k-ϵ model is one of the best models for atmospheric flow modelling. There are some experiments done to study forest effects on airflow [12]. These experimental studies will be used to validate numerical simulations.

2.5.3 Large-Eddy Simulation

In RANS all turbulent scales are modelled. To more accurately account for the effects of turbulence, the large scale eddies can be resolved, this is Large-Eddy Simulation (LES). Rather than time-averaging the governing equations (as done with RANS), a 'spatial filtering' is made to separate turbulent eddies depending on their length scale. For high Reynolds numbers the small eddies are predictable [8]. However, they are computationally expensive to resolve, therefore they are modelled. LES is more time consuming than RANS, but it is able to capture the anisotropic behaviour of the large eddies which is ignored by RANS.

2.5.4 Turbulence Intensity

The turbulence of a flow may be quantified using turbulence intensity (TI). It is a dimensionless parameter, which is defined as the ratio of the fluctuations of the flow to the mean velocity field.

$$I = \frac{v'}{\bar{v}} \tag{2.17}$$

where v' and $\bar{v}$ denote the velocity fluctuations and mean velocity, respectively. In RANS, the fluctuations may be estimated by using the turbulent kinetic energy, k, resulting in Eq. 2.18 [11].

$$I \approx \frac{\sqrt{\frac{2}{3}k}}{\bar{v}} \tag{2.18}$$

For CFD simulations of turbulent flow, a specified TI can be used as a boundary condition for the inlet of the domain. This is usually done either to speed up the convergence, or in order to achieve a certain turbulence. For example, when using the k-ϵ model, both k and ϵ can be calculated from a specified TI.

2.6 Atmospheric boundary layer

In the lowest part of the atmosphere lies the Atmospheric Boundary Layer (ABL). This is the part of the atmosphere where most transport processes happens, processes like heat or momentum exchange. One of the most characteristic traits of the ABL is the turbulence. Where the turbulence disappears is often defined as the top for the ABL. The wind speed at the top of the ABL is equal to the wind speed of the free atmosphere.

The speed at the ground reduces to zero with a logarithmic velocity profile. Due to the surface friction, the changes close to the surface are fast [13]. The turbulence causes the influence of surface friction and heating to quickly be transferred to the entire ABL. At the bottom 10% of the ABL lies the surface layer. In this layer the turbulence is fully developed [14]. This layer is influenced by the surface roughness like grass and trees. At the very bottom, below the surface layer, is a laminar layer with a characteristic length, the so-called surface roughness length, y_0. Depending on terrain, y_0 may vary between a millimeter and close to a meter.

The thermal stratification determines the height of the ABL and the scales of the turbulence. During the day the boundary layer height increases when surface heating results in a large thermal motion. In the late afternoon the height can be up to 3000 m. The stratification is unstable. During the night the stratification is stable. The cooling contributes to suppression of turbulent scales and the height decreases. At night the top of the layer can lie as low as 100 m above the ground. When the wind is strong and during the afternoon the stratification can be said to be neutral. In the neutral Atmospheric Boundary Layer, see Fig. 2.6, the turbulence is generated by the wind gradient, not by surface heating [13].

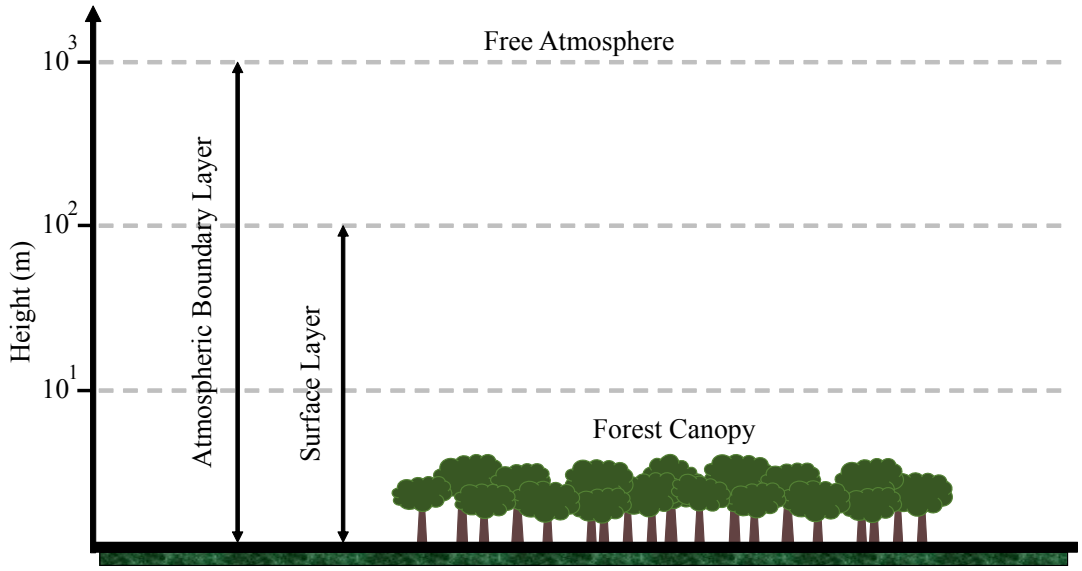

Figure 2.6: The atmospheric boundary layer, with scales typical for near-neutral stability.

2.7 Modelling the forest

In this study, a forest resides at the bottom of the ABL and affects the flow. The forest can be treated as a drag body force acting on the fluid. It is therefore introduced as a sink term in Eq. 2.11, i.e. an external force retarding the flow. Mathematically it is given by

$$S_u = -C_D a_f |\bar{\mathbf{v}}| \bar{v}_i \tag{2.19}$$

where S_u, C_D, a_f and $|\bar{\mathbf{v}}|$ denote the sink term, the drag coefficient, the leaf area density (LAD) and the magnitude of the mean flow velocity vector, respectively. In accordance with Shaw and Schumann [15], C_D is equal to 0.15. The leaf area density (a_f) is the area of leaves per unit volume and thus have the dimension [m^{-1}]. The LAD profiles used in this study can be seen in Fig. 3.3. Furthermore, LAD profiles might vary depending on forest canopies, therefore a useful cumulative measure is the leaf area index (LAI). It is defined as

$$\mathrm{LAI} = \int_0^h a_f \, dy \tag{2.20}$$

where h is the tree height.

The turbulent kinetic energy and its rate of dissipation are also affected by the forest. When the mean flow collides with the forest elements, wake turbulence is generated, thus the TKE increases [16]. Turbulent dissipation grows because the eddy length scales shrink in this region due to the generation of wakes. This process can be described as a 'short-circuit' [17] of the energy cascade, see section 2.3. The mentioned mechanisms are reflected in the sink/source terms given by

$$S_k = C_y \left(\beta_p |\bar{\mathbf{v}}|^3 - \beta_d |\bar{\mathbf{v}}| k \right) \tag{2.21}$$

$$S_\epsilon = C_y \left(C_{\epsilon 4} \frac{\epsilon}{k} \beta_p |\bar{\mathbf{v}}|^3 - C_{\epsilon 5} \beta_d |\bar{\mathbf{v}}| \epsilon \right) \tag{2.22}$$

where S_k, S_ϵ are sink/source terms; β_p, β_d, $C_{\epsilon 4}$ and $C_{\epsilon 5}$ are model coefficients and C_y is an effective drag coefficient. β_p is related to the conversion of mean flow kinetic energy to TKE, and β_d relates to the short-circuit process [12]. For simplicity the effective drag coefficient is introduced, and is defined as $C_y = C_D a_f$. By introducing the sink/source terms S_u, S_k and S_ϵ, the transport equations for momentum, turbulent kinetic energy and turbulent dissipation rate (Eqs. 2.11, 2.15 and 2.16, respectively) can be modified

for forest modelling as

$$\frac{\partial(\bar{v}_j\bar{v}_i)}{\partial x_j} = -\frac{1}{\rho}\frac{\partial \bar{p}}{\partial x_i} + \frac{\partial}{\partial x_j}\left[\nu\frac{\partial \bar{v}_i}{\partial x_j} + \nu_t\left(\frac{\partial \bar{v}_i}{\partial x_j} + \frac{\partial \bar{v}_j}{\partial x_i}\right) - \frac{2}{3}\delta_{ij}k\right] + S_u \quad (2.23)$$

$$\bar{v}_j\frac{\partial k}{\partial x_j} = \nu_t\left[\frac{\partial \bar{v}_i}{\partial x_j} + \frac{\partial \bar{v}_j}{\partial x_i}\right]\frac{\partial \bar{v}_i}{\partial x_j} + \frac{\partial}{\partial x_j}\left[\left(\nu + \frac{\nu_t}{\sigma_k}\right)\frac{\partial k}{\partial x_j}\right] - \epsilon + S_k \quad (2.24)$$

$$\bar{v}_j\frac{\partial \epsilon}{\partial x_j} = \frac{\epsilon}{k}C_{\epsilon 1}\nu_t\left[\frac{\partial \bar{v}_i}{\partial x_j} + \frac{\partial \bar{v}_j}{\partial x_i}\right]\frac{\partial \bar{v}_i}{\partial x_j} + \frac{\partial}{\partial x_j}\left[\left(\nu + \frac{\nu_t}{\sigma_\epsilon}\right)\frac{\partial \epsilon}{\partial x_j}\right] - C_{\epsilon 2}\frac{\epsilon^2}{k} + S_\epsilon \quad (2.25)$$

In the sink/source terms S_k and S_ϵ, the coefficients are weights to the different mechanisms. The values most suitable for the coefficients varies in literature. In Tab. 2.3 four different sets of parameters are listed, which are compiled from different studies [12; 16; 17; 18; 19]. Throughout this report these sets of parameters are referred to as the 'canopy models', and individual models are called by their author's name.

Table 2.3: Four sets of canopy model coefficients for the sink/source terms S_k and S_ϵ [12]. Each set comes from a previous study, whose author is seen in the model column.

Model	β_p	β_d	$C_{\epsilon 4}$	$C_{\epsilon 5}$
Green	1.0	4.0	1.5	1.5
Sanz	1.0	5.1	0.9	0.9
Liu	1.0	4.0	1.5	0.6
Svensson	1.0	0.0	1.95	0.0

2.7.1 Canopy model basis descriptions

The parameters as mentioned in the previous subsection, are gathered from different studies. The Svensson model is derived from a study assuming a canopy height of 2.5 m, a drag coefficient C_D of 0.3 and a Plant Area Density (PAD) of 2.1 m^2/m^3. PAD differs from LAD in that PAD takes into account the trees and not just the leafs. This makes it possible to evaluate deciduous forest during winter when they do not have any leaves. The height of the studied volume was 134.25 m and it had a finite length of 3700 m [19].

Green's model is from a study performed on a volume with the entrance size being 1.07 m high and 1.53 m wide. The total length of the volume was 5.0 m and the tests were conducted at low wind speeds. The trees that were used in the study had a height of about 200 mm and were shaped like a cone with a base diameter of 40 mm. Around 700 of these trees were placed approximately 2.0 m downstream from the

entrance. Lastly C_D was set to 0.6 which was presumed to be a characteristic value for the forest trees [18].

The third model named Liu is derived from studying the flow through a volume with a width of 2.4 m, a height of 1.5 m and a length of 25 m. This volume was used to study a "forest" with a height of 0.15 m. The drag coefficient was derived from spruce forest at 0.3 and the LAD used can be seen in Tab. 2.4. The study was also conducted at wind speeds between 0.7 m/s and 16 m/s [17].

Table 2.4: Leaf Area Density distribution used in Liu's study [17].

y (m)	LAD (m^2/m^3)
0.141-0.150	28.0
0.111-0.140	38.0
0.081-0.110	53.5
0.051-0-080	55.5
0.021-0.050	57.5
0.000-0.020	6.0

The last constants named Sanz were provided by studying canopies ranging between 0.12 m to 23 m with a LAI between 2 to 10 m^2/m^2. The C_D used in the study ranged from 0.1 to 0.3 [16].

3

Method

The main portion of this project was performed with CFD simulations using the STAR-CCM+ software. Any CFD simulation consists of three main parts: A pre-processor, solver and post-processor. In the first part, the geometry, physics, boundary conditions and mesh settings are set up. The physics and forest modelling are discussed in the theory chapter, while the geometry and mesh are described in detail in section 3.1. In the second part called the solver, the software solves the equations. After finishing the simulation, the software enters the post-processing step, where the data and results are handled. The point where the simulation is finished, called stopping criteria, is determined by the user. It can be a certain amount of time steps or when the solution is converged. The solution is converged when the corresponding residuals are smaller than 10^4.

The data of interest may be presented directly in plots or tables, further processed, or exported for use in any external software. In this case several scripts written in MATLAB were used to draw plots of the exported data.

The simulations for this project are divided into steps with increasing complexity. At first, the domain for the simulation was set up without any forest or a wind turbine. The forest was then added using four different canopy models. For each model, the simulation was repeated for both 'sparse' and 'dense' forest leaf area densities, and for four different velocities. By comparing the results to LES data, the most well suited canopy model was found. This model was then used in the final step of the simulations, where a wind turbine was implemented in an adjusted geometry.

3.1 Setting up the simulations

Before performing any kind of simulation, the simulation needs to be set up. This includes the simulated volume, objects that reside in the volume, boundary- and physics conditions and much more. This set up stage is the part of the simulation that takes up the most man-hours. This is in order to reach a good result with a small number of simulations. The computational costs can increase drastically when more complex or larger simulations are needed, it is therefore wasteful to run a lot of poorly set up simulations. The main steps for how the simulation was set up for the two different volumes will be explained in the following sections.

3.1.1 Domain & boundary conditions

When deciding the size of the domain for the simulations with the forest, the main goal was to adapt the size to the most standard wind turbine provided by the NREL. The reference used was a 5-MW Wind turbine, and in Tab. 2.1 the main properties that are interesting for sizing the project are presented.

The geometry size was chosen to be large enough to simulate the airflow over the reference wind turbine. The hub height is 90 m and adding the radius of the rotor puts the total height of the wind turbine at 153 m. This height was used when deciding the total height of the domain. The boundary condition used for the sky of the domain was set to symmetric. Due to the implementation of symmetric boundary conditions and with regards to the turbine height, the simulated domain height was set to 300 m, see section 2.4.1 for an explanation of the symmetry condition.

For the inlet and outlet sides of the domain, the periodic boundary condition was chosen. Because of this, the length of the domain was set to 600 m which was enough to see the results of the fully developed flow without unnecessarily increasing the computational time. The streamwise length was set to be the longest in order to more easily visualise and study the flow.

The sides of the domain was also set as periodic. The periodic boundary conditions make the simulation more accurate by eliminating the effects the sides would have upon the computational domain if a 'wall' type boundary was used. In others words the periodic boundary condition makes it possible to imitate a wider forest. With this in regard, the width of the domain was set to 300 m because of the rotor diameter of the wind turbine being 126 m. The full domain can be seen in Fig. 3.1.

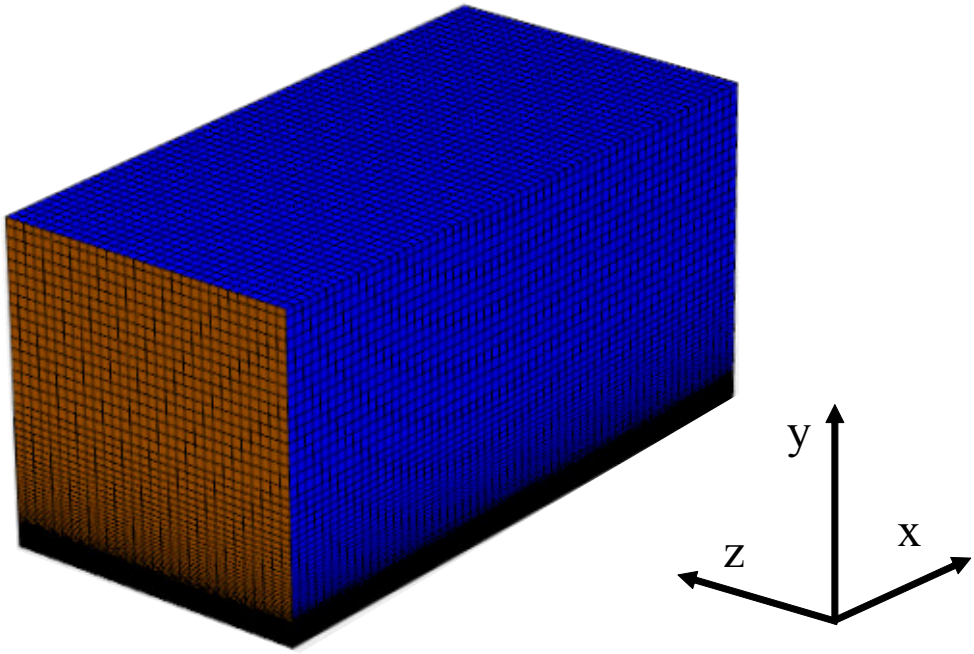

Figure 3.1: An overview of the geometry used in the simulation with and without the forests.

The ground of the domain was set as a wall due to the air not being able to pass trough it, the no-slip condition also applies here. The boundary conditions used are summarised in Tab. 3.1.

Table 3.1: Boundary conditions for the domain.

Boundary	Inlet/outlet	Ground	Sky	Sides
Condition	Periodic	Wall	Symmetry plane	Periodic

3.1.2 Mesh

Looking at Tab. 3.2 the main settings for the computational grid are displayed. The prism layer named in the table is an area of the domain close to the bottom side where the cells are refined. This means that the cell heights in this region are lower than the main bulk cell height. The reason behind this is because there are areas in

the computational domain which are of special interest. The bottom wall is the area where most of the turbulence is generated by the velocity gradient. By refining the cell size close to the wall the simulation is able to capture the turbulence well which accordingly provides more accurate results. As seen in Fig. 3.1, a gradual increasing height of the cells represent the prism layer. Although smaller cells close to the wall is preferable, the computational time is increased with added cells. To counteract this, a gradually increasing cell size is placed with the height increasing by 20% for each cell moving upwards. The cells need to be gradually increased because if the size increases drastically from one cell to another this may reduce the accuracy of results. The cells are each represented by a cube with the outside faces seen in Fig. 3.2, representing a close up of the prism layer.

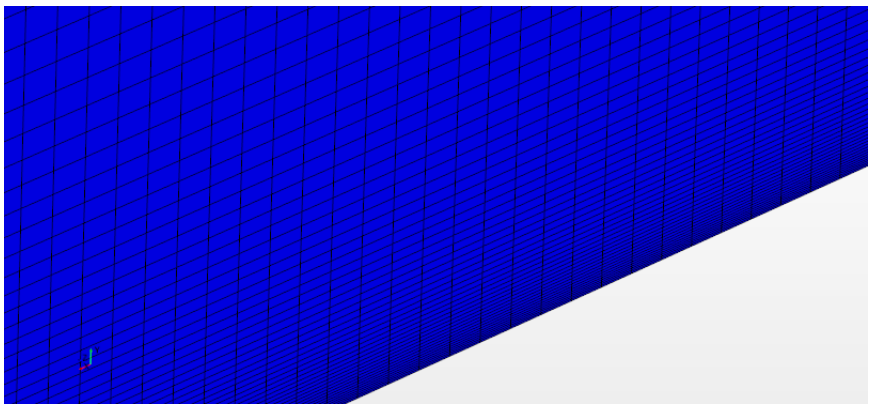

Figure 3.2: A close up of the prism layer showing an increase in cell height when moving up from the bottom wall of the domain.

The height of the smallest bottom cells in the prism layer was set to 0.4 m because of the need to have lower height at the bottom but without increasing the computational time drastically. The height was then gradually increased in 50 cell layers up to 125 m. The transition from the prism layer to the main cell size was made such that the size difference was the same as between cells in the prism layer. The base size cells are located at the top of the volume. The sides of each have a length of 10 m. The table containing settings for the mesh can be found in Tab. B.1 in Appendix B.

Table 3.2: Settings and properties for the (automated) mesh in STAR-CCM+.

Setting	Value
Base size	10 m
Number of prism layers	50
Prism Layer Near Wall Thickness	0.4 m
Prism Layer Total Thickness	125 m
Maximum Cell Size	10 m
Surface Growth Rate	1.3

For the simulations with and without forest, employing a prism layer near the wall region increases the accuracy of the results. The area near the rotor blades and the wake were included in the prism layer and needed no further local refinement to capture the turbulence occurring there. To find the needed refinement for the mesh, a test for mesh independence was performed. This meant running the simulation a couple of times with decreasing refinement to see if the results would differ. As long as the results would remain the same while reducing the number of cells, this only meant a decrease in computational time which is always desirable.

3.1.3 Mass flow rate

The mass flow rate at the inlet was estimated by assuming a logarithmic wind profile within the atmospheric boundary layer. It was estimated as

$$\bar{v}_1 = \bar{v}_{1,ref} \frac{\ln(y/y_0 + 1)}{\ln(y_{ref}/y_0 + 1)} \tag{3.1}$$

where $\bar{v}_1$, $\bar{v}_{1,ref}$, y, y_{ref} and y_0 denote the mean streamwise velocity, reference wind speed, vertical position, reference height and surface roughness length, respectively. This profile features two reference values: the wind speed $\bar{v}_{1,ref}$ at the reference height y_{ref}. The reference height was taken as the NREL turbine's hub height, $y_{ref} = y_{hub} = 90$ m. The wind speeds of interest (5, 8, 12 and 20 m/s) were used as values for $\bar{v}_{1,ref}$. The surface roughness length used was $y_0 = 2$ cm, which is only slightly lower than a value used for open farmland [14].

The mass flow rate could subsequently be calculated as

$$\dot{m} = \rho A_{in} U_b \tag{3.2}$$

where $\dot{m}$, ρ, A_{in} and U_b represent the mass flow rate, the density of air, inlet area and the bulk velocity, respectively. The density of air was taken as ρ = 1.18 kg/m^3 and the inlet area A_{in} = 9 $\times$ 10^4 m^2. The bulk velocity was calculated as

$$U_b = \frac{1}{|b-a|}\int_a^b \bar{v}_1 dy \tag{3.3}$$

where a = 0 m and b = 300 m. Time was saved by estimating the mass flow rate in this manner, which would otherwise have had to be guessed and thereafter controlled to yield an acceptable $\bar{v}_{1,hub}$. The distinction between $\bar{v}_{1,hub}$ and $\bar{v}_{1,ref}$ is that the former is the actual simulated streamwise velocity at y_{hub}, while the latter is a tool used for estimating the mass flow rate. Proceeding, the mass flow rates may be referred to by their corresponding reference wind speed $\bar{v}_{1,ref}$.

3.1.4 Leaf Area Density Profiles

In this section the leaf area density (LAD) and the leaf area index (LAI) are referred to. Their definitions can be found in section 2.7. Two different forests were simulated, one 'sparse' and one 'dense'. The forests were represented by their respective LAD profile, a_f. Both profiles are illustrated together in Fig. 3.3. The LAI corresponding to the sparse and dense profiles were 2.8 and 5.8, respectively. In other words: Cumulatively and compared to the sparse forest, the leaf area density of the dense forest is more than twice as large. The LAI values that were used are approximately typical values used for a deciduous forest [15; 20]. The canopy height was taken as h = 20 m. In order to assess the effect of the forest on the flow, simulations were also done without the forest.

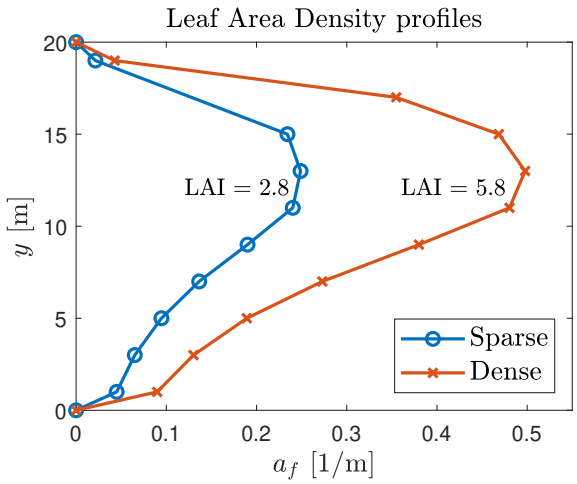

Figure 3.3: The two different leaf area density (a_f) profiles used for the simulations. The leaf area index (LAI) is 2.8 and 5.8 for the sparse and dense profile, respectively.

3.2 Evaluation of different canopy modelling

In order to save resources, the most appropriate canopy model, see Tab. 2.3, for the prescribed LAD had to be found. In order to compare how well the different canopy models fit the forest parameters, only one mass flow rate was simulated for each model. The results were then compared to data from a previously conducted Large-Eddy Simulation (LES) made with the sparse forest. For the LES, the spatial dimensions of its domain were 10 km, 1 km and 1 km in the streamwise, vertical and spanwise direction, respectively. The compared results were the distribution of turbulent kinetic energy and the velocity profile of the flow, both as functions of height. Once the most accurate model was found, further simulations were run at both higher and lower flow rates. Since this was done just once for all four models, a lot of resources were saved. The canopy models have been curve fitted to different experimental data, and may or may not be well suited for the parameters used in our simulations. If this is the case they might even diverge and a fully developed solution with small residuals can not be found, see Fig. A.1 in Appendix A.

3.2.1 Curve Fits

To provide data for the curve fits, four simulations were conducted, one for each canopy model. The mass flow rate used at the inlet was set to 9.3 $\times$ 10^5 kg/s. Note that this mass flow rate was not calculated using the method explained in section 3.1.3, it was set manually. The rate was such that $\bar{v}_{1,hub} \approx 8$ m/s for each model, which coincided with the $\langle \bar{v}_1 \rangle_{hub}$ of the LES. The notation $\langle \bar{\cdot} \rangle$ is LES terminology for a spatially filtered and time averaged quantity. The LES data had been conducted with the sparse LAD profile, therefore the sparse profile was used for evaluation of the canopy model simulations as well. The mean streamwise velocity profiles for both the LES and the canopy models were curve fitted to a power exponent function defined as

$$\bar{v}_1(y) = \bar{v}_{1,hub} \left(\frac{y}{y_{hub}} \right)^{\alpha} \tag{3.4}$$

where α is the power exponent being fitted. It is called the shear exponent and is used in wind engineering as a measure of much turbulence can be caused by the wind shear [21; 22]. MATLAB's built-in Curve Fitting Tool, 'cftool', was used for the purpose of making the curve fits, which were made in a least mean square sense. Only the part of the velocity profiles within the rotor area, $y \in$ [27 m, 153 m], were used for curve fitting.

3.3 Implementing the wind turbine

The last part of the project included implementing a wind turbine which was modelled by using STAR-CCM+'s built-in model 'virtual disk'. The 1D momentum method was used to model the effects of the wind turbine. It requires performance curves of a wind turbine, which means the power and thrust coefficient as functions of the wind velocity. The disc was implemented by defining the its geometry and the inlet flow including its direction and velocity. Components of the geometry include the height, radius and blade thickness. The geometry data was based on the NREL 5-MW wind turbine, see Tab. 2.1. The blade thickness was determined by looking at the mesh size near the rotor blades, as the thickness must be at least one cell wide. Performance data for the turbine was imported based on previous data, see Tab. B.2 in Appendix B. The inlet flow for the disc was defined as a circular velocity plane with a radius of 70 m, located 2.5 m upstream of the actuator disc location. The rotor speed was calculated by linear interpolation of the turbine's rotational speed and evaluating it at the wind velocity at hub height.

The simulations with the wind turbine were different from the ones with only the forest, see 3.1.1 for the old domain. One of the changes required was a different geometry. The height and the width remained the same as in the previous simulations, but the length needed to be increased. This was because of the inlet-outlet boundary condition needed during these simulations. The reason behind the inlet-outlet boundary condition was the effect of the wind turbine. Using a periodic boundary condition would let the wake behind the turbine go in as inlet flow to an additional turbine in the time step. Because of these facts an inlet-outlet boundary condition needed to be used and the length of the geometry was set to 2000 m, as seen in Fig. 3.4. The boundary conditions for the wind farm geometry can bee seen in Tab. 3.3. Note that the sides are set as symmetric, but that is only because the STAR-CCM+ requires it. An additional interface between the sides was made for them to act as periodic boundary condition similar to the previous domain.

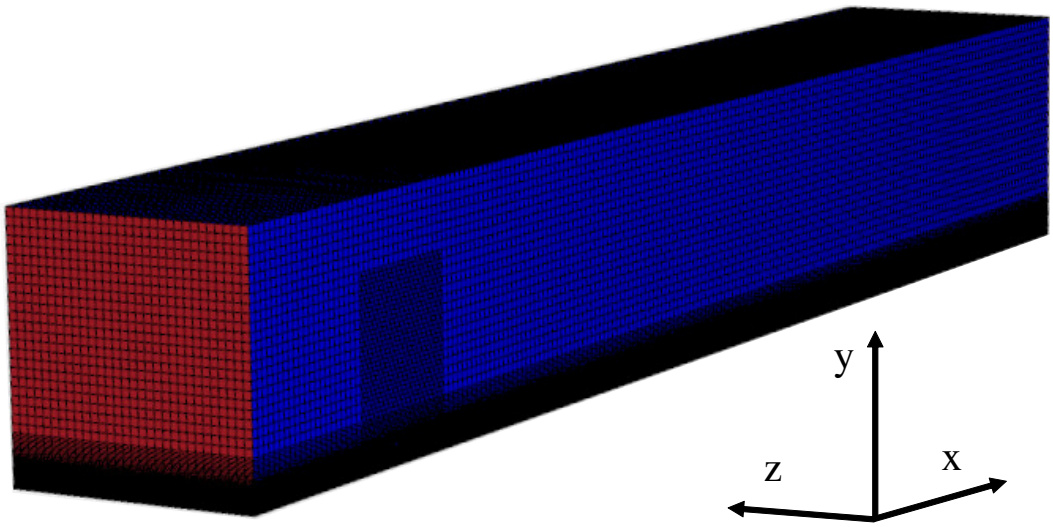

Figure 3.4: An overview of the geometry used in the simulation with the wind turbine.

Table 3.3: Boundary conditions for the domain including a wind turbine.

Boundary	Inlet	Outlet	Ground	Sky	Sides
Condition	Velocity Inlet	Pressure Outlet	Wall	Symmetry	Symmetry

The mesh used for the domain with the wind turbine was largely unchanged from the

previous simulations, see Tab. 3.2. However, local refinements were added around the disc and in the wake region. Both refinements were defined as cylinders with a radius of 90 m. The disc refinement had a length of 20 m, centred around the turbine and with a refinement 10% of the base size. The wake refinement had a length of 1705 m, placed behind the turbine and extending to the end of the domain, and with a refinement 25% of the base size. In addition to these changes, the prism layer total thickness was reduced from 125 m to 60 m. This was done because the mesh was already very refined in the wake region, and computational time and power could be saved. Figure 3.5 shows the mesh including the refinements.

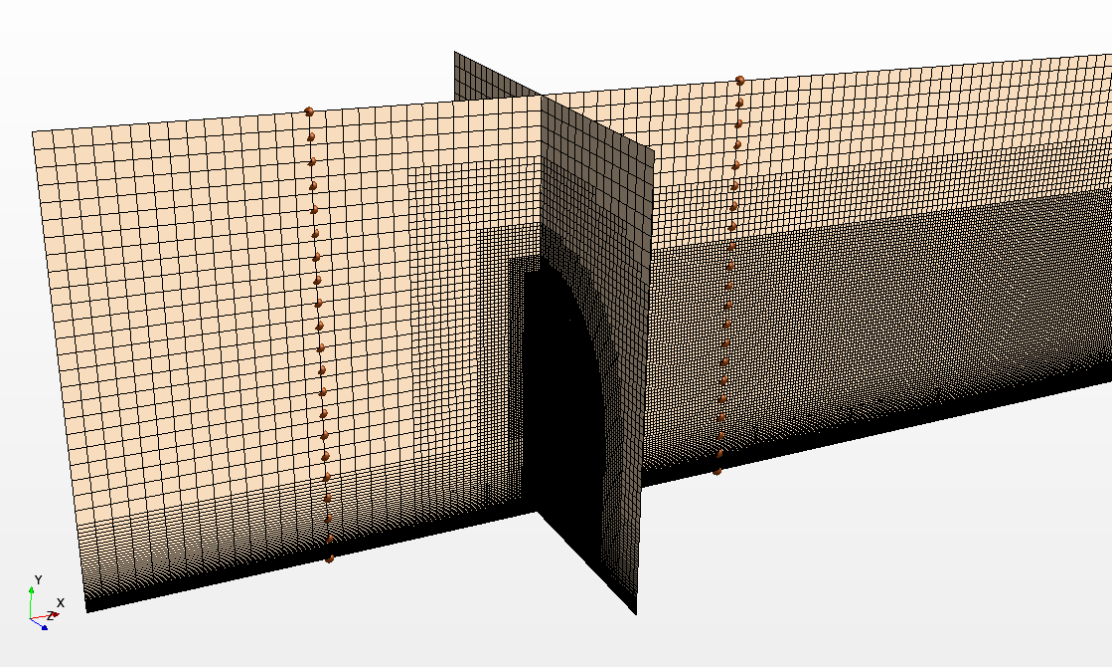

Figure 3.5: An overview of the mesh used in the simulation including the wind turbine modelled as actuator disc.

3.4 Initial conditions

For both domains, initial conditions were given for the flow velocity vector, the turbulent kinetic energy and the turbulent dissipation rate. The initial conditions for k and ϵ were defined as

$$k = (I\bar{v}_{1,ref})^2 \tag{3.5}$$

$$\epsilon = \frac{u_\tau^3}{\kappa(y + \Delta)} \tag{3.6}$$

where I, $\bar{v}_{1,ref}$, κ, u_τ, Δ denotes turbulence intensity, reference wind speed, the von Kármán constant, the wall friction velocity and a small height, respectively. The turbulence intensity was set to $I = 0.1$. The von Kármán constant was set to $\kappa = 0.42$. The small height, $\Delta = 1 \times 10^{-13}$ m was added to the denominator in Eq. 3.6 to prevent ϵ from going to infinity near the wall. The wall friction velocity was estimated as

$$u_\tau = \frac{\kappa\bar{v}_{1,ref}}{\ln\left(y_{ref}/y_0 + 1\right)} \tag{3.7}$$

The logarithmic profile defined in Eq. 3.1 was used as initial condition for mean streamwise velocity, $\bar{v}_1$. The vertical and spanwise components of the mean velocity vector were both set to zero.

4

Results

In this chapter, the results are presented in the order of which they are obtained. The interest in this study is the vicinity of the wind turbine. Therefore, only the lowest 300 m of the domain is presented. In section 4.1 the result of the simulations with the different canopy models are displayed. Following this is section 4.2 where the impact of the forest is declared. Section 4.3 presents the result of the wind turbine and in the last section the sources of error are discussed.

4.1 The canopy models

The results from the curve fitted power exponents described in section 3.2.1 are presented in sections 4.1.1 - 4.1.4. These results are based on four simulations with the all the canopy models: Sanz's, Green's, Svensson's and Liu's model, which are described in section 2.7. The exponents are compared to that of the Large-Eddy Simulation (LES). Furthermore, the turbulent kinetic energy of the canopy models and the LES are presented and compared.

Lastly, the results of 24 additional simulations are presented, featuring three canopy models for four mass flow rates in the sparse and the dense forest. These results are used to explore how the canopy models' may affect the mean flow and turbulent kinetic energy.

4.1.1 Fitting of power exponents

Figure 4.1a illustrates the data used for the power exponent fits, which in turn can be viewed in Fig. 4.1b. In line with a previous study [12], all the canopy models overestimate the mean streamwise velocity within the forest region ($y \leq h$ = 20 m), as is seen in Fig. 4.1a. The results presented in Tab. 4.1 shows that Sanz's model power exponent is closest to that of LES. Note that Sanz's power exponent is only marginally better than Green's. Furthermore, Svensson's shear exponent (α) is overestimated by 12%, which is comparable to Sanz's which is underestimated by 7%. The high values for the coefficient of determination, R^2, indicate that the power exponent functions make good fits within the rotor area for the canopy models and the LES. Moreover, looking at the values for $\bar{v}_{1,hub}$, it is suggested that the mass flow rate is set too low, because no canopy model had a $\bar{v}_{1,hub}$ as high as LES.

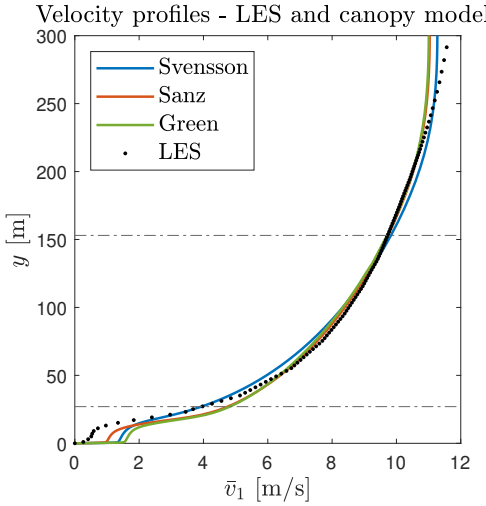

(a) The mean streamwise velocities $\bar{v}_1$ for the LES data together with the simulated canopy models. The horizontal dashed lines mark the rotor area which was the portion of data used for curve fitting.

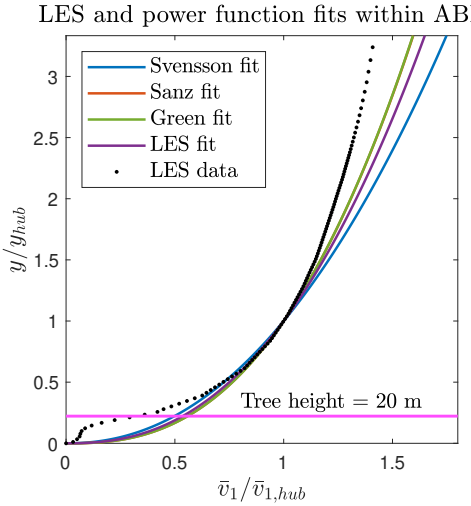

(b) The LES data together with the curve fitted power exponent functions. Note that Green's and Sanz's fitted functions are practically on top of each other. Values are normalized with the hub height, y_{hub}, and the mean streamwise velocity at the hub, $\bar{v}_{1,hub}$.

Figure 4.1: The data used for the curve fits (left), and the resulting power function fits (right) together with the LES data. The magenta horizontal line indicates the tree height.

Looking at Tab. 4.1, no results are displayed for Liu's model. The simulations using Liu's model did not converge, that is to say the corresponding residuals did not fulfil the stopping criteria: being smaller than 10^{-4}. The reasons for this are discussed further in section 4.1.2. Proceeding, Liu's model is not used as a candidate model.

Table 4.1: The power exponent α for different canopy models, along with $\bar{v}_{1,hub}$ which differ only slightly between the models. R^2 is the coefficient of determination, which is used to evaluate how well the power exponent functions fit to the data. Among the canopy models, Sanz's α is closest to that of the LES.

Model	α	$\bar{v}_{1,hub}$ [m/s]	R^2
LES	0.4151	8.2076	0.9612
Svensson	0.4639	7.9577	0.9858
Green	0.3872	8.0034	0.9981
Liu	-	-	-
Sanz	0.3878	8.0719	0.9955

4.1.2 Liu's model and convergence

Out of the four canopy models used only three converged with this project's settings. A non-converging result means that the residuals do not tend towards smaller numbers and means that a model isn't fitted well to the parameters used. This is just a result of using models. They are meant to simplify some aspects of a system, such as approximating a term in an equation like the Reynolds stresses. What this means in practice is that a certain model might be tuned well for a certain type of flow but not at all suitable for another.

This is exactly what was observed within Liu's model used in this project's simulations which was mentioned as a potential issue in section 3.2, see Fig. A.1 in Appendix A. The model seemed to be non-converging even when using a heavy under-relaxation factor. This result, while unexpected, is not surprising. The four models used were developed for other studies of flow such as over miniature forests in wind tunnels. Running experiments on a smaller scale and tuning the model to fit doesn't necessarily mean that a scaled up simulation will run poorly however.

What ultimately determines how a particular flow behaves is the Reynolds number (Re). As long as it is kept close to that of the simulation or experiment used to develop the model, chances are that the model will work. Some models can be more sensitive than

the others though, which was noticed in some of the converging models taking longer to converge than the others when using certain parameters. Looking at the formula for the Reynolds number, see Eq. 2.3, it can be seen that if the scale is reduced, such as when doing an experiment in a wind tunnel, the velocity must increase in order to keep the flow properties (Re) the same. Because wind tunnels can not achieve such flow rates, and Liu's model was tuned for one of these experiments [12; 17], it can be seen why it might not be as well suited for a large scale simulation like the one used in this project. If it had been, it must have been tuned to a wind tunnel experiment of unimaginably high flow rates.

4.1.3 Comparing turbulent kinetic energy

The Turbulent Kinetic Energy (TKE) is another decision factor for assessing which canopy model best produces results close to the LES. As seen in Fig. 4.2, it is clear that Sanz's model most closely follows the TKE profile of the LES, and it produces the closest value of maximum TKE, as displayed by Tab. 4.2. All canopy models overestimate the TKE which is due to the presence of the forest. However, Green's model does this to a much larger extent than the other two models. Green's model redeems this shortcoming by best predicting the vertical position of the maximum TKE.

Table 4.2: The value and vertical position (as a multiple of the tree height, h) of maximum turbulent kinetic energy for the different canopy models and the LES.

Model	Max TKE [J/kg]	Vertical position [m]
LES	3.4793	2.1500 h
Svensson	4.1376	1.2250 h
Green	5.3895	1.7750 h
Sanz	3.7909	1.6375 h

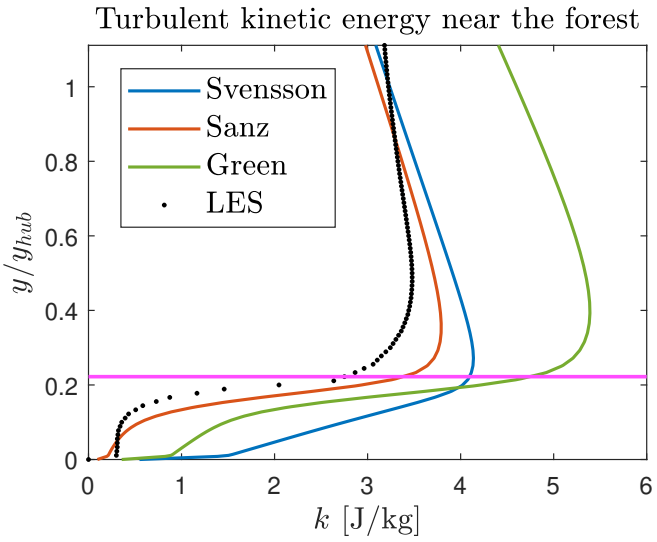

Figure 4.2: The TKE for the canopy models and the LES. The horizontal magenta line marks the tree height, h = 20 m. The values on the vertical axis are normalized with the hub height y_{hub} = 90 m.

Svensson's model fails to excel in either comparison (α or TKE), therefore it is eliminated. Green's and Sanz's models have nearly the same power exponent α. Sanz's model is superior in predicting maximum TKE at the cost of slightly underestimating the vertical position of maximum TKE, more so than Green's model. Green's model is a strong candidate, however, Sanz's model is the model of choice for this study because of the observations made in this section and section 4.1.1.

4.1.4 Evaluating Sanz's model

In this section the reference wind speed ($\bar{v}_{1,ref}$) is frequently used, which is defined in section 3.1.3. The reader is reminded that it is a tool to estimate mass flow rate, as opposed to $\bar{v}_{1,hub}$ which is the actual simulated mean streamwise velocity at hub height. The results in sections 4.1.1 and 4.1.3 justify the choice of Sanz's model for mass flow rates such that $\bar{v}_{1,hub} \approx 8$ m/s. However, it is yet unclear if Sanz's model is a valid choice for the other relevant mass flow rates ($\bar{v}_{1,ref}$ = 5, 8, 12 and 20 m/s). Because the LES data is limited to only one mass flow rate, an assumption is made in order to progress: The LES data can be scaled. This assumption is valid to make because the flow of the LES is fully turbulent with a high Reynolds number, thus the shape of any simulated profile is invariant to change in mass flow rate. For the sparse forest, this assumption

allows for evaluations of the canopy models at other mass flow rates by normalizing the data.

In Fig. 4.3 the mean streamwise velocity profiles are shown for four different mass flow rates with the sparse forest. Normalizing the velocity profiles with their corresponding $\bar{v}_{1,hub}$ yields very similar profiles. These findings suggest that for a sparse forest, Sanz's model is the most suitable choice for all mass flow rates.

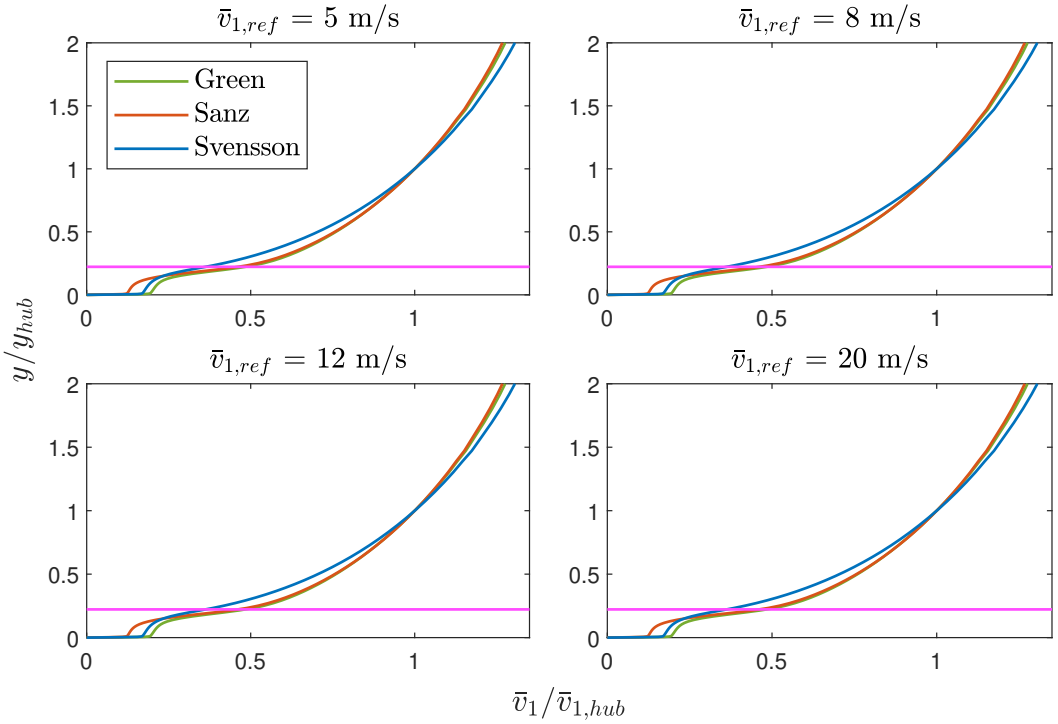

Figure 4.3: Mean streamwise velocity profiles for the three converged canopy models, at four different simulated mass flow rates for the sparse forest. When normalized, the velocity profiles are seemingly unaffected by the change in mass flow rate. The magenta horizontal lines represent the tree height.

The same type of comparisons are also made using the dense forest profile, and again no clear variation in the shapes can be found between the different mass flow rates. Due to the repetitiveness of these figures, the reader is referred to Appendix A to see the four results side by side. However, one of four results is illustrated in Fig. 4.4, featuring the normalized velocity profiles for the mass flow rate corresponding to $\bar{v}_{1,ref}$ = 8 m/s. Comparing the results for the dense and sparse forest, the canopy models behave similarly except for close to the wall, under the tree line (h/y_{hub} = 0.22). In

that region Green's and Svensson's model behave differently: Green's model predicts a greater retardation due to the dense forest than Svensson's model.

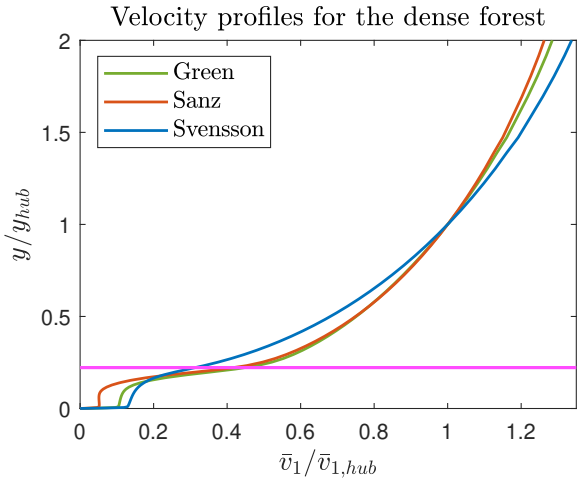

Figure 4.4: The three converged canopy models' mean streamwise velocity profiles for the dense forest. The mass flow rate corresponds to $\overline{v}_{1,ref}$ = 8 m/s. The magenta horizontal line represents the forest height.

It should be noted that no results have yet been presented that directly support Sanz's superiority among the canopy models for the dense forest. Looking at Fig. 4.5, it is clear that Sanz's model is unique in underestimating the turbulent kinetic energy for the dense forest relative to the sparse forest. However, this prediction is not consistent with results of a previous study by Nebenführ and Davidson [20]. The TKE is expected to increase for the dense forest, thus a shortcoming of Sanz's model is found.

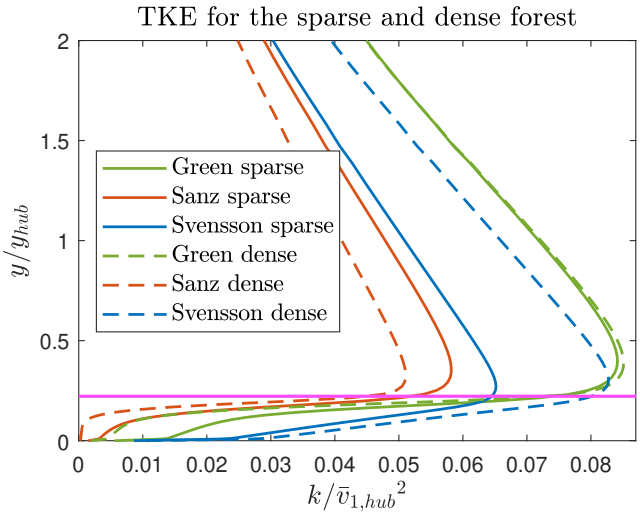

Figure 4.5: The three converged canopy models' turbulent kinetic energy for the dense forest and the sparse forest. The mass flow rate corresponds to $\bar{v}_{1,ref}$ = 8 m/s. The magenta horizontal line represents the forest height. Values are normalized with the hub height (y_{hub}) and the mean streamwise velocity at hub height ($\bar{v}_{1,hub}$).

4.2 Impact of the forest canopies on the air flow

In this section the effect of the forest on the flow properties $\bar{v}_1$ and TKE are presented. As shown in section 4.1.4, the profiles are similar when normalized for both streamwise velocity and turbulent kinetic energy. For practical reasons, rather than showing four nearly identical profiles (one for each simulated mass flow rate), only the results from simulations with the mass flow rate corresponding to $\bar{v}_{1,ref}$ = 8 m/s are shown here. The presented results are from simulations using Sanz's canopy model.

As illustrated in Fig. 4.6a, a prominent effect of the forest is the shearing of the velocity profiles. Furthermore, the (normalized) mean flow for the dense forest is retarded to a larger extent than that of the sparse forest, and the most notable difference is seen under the tree line. Within the rotor area hardly any difference can be seen. Qualitatively, these results agree with a previous study by Nebenführ and Davidson [20], which is based on Large-Eddy Simulations and with similar conditions. For a dense forest, this is the strongest support found for Sanz's model. It does not necessarily show that Sanz's model is the most suitable canopy model to describe the mean flow for a dense forest. However, it does suggest that Sanz's model at least correctly captures the qualitative differences of the mean streamwise velocity between a sparse and a dense forest.

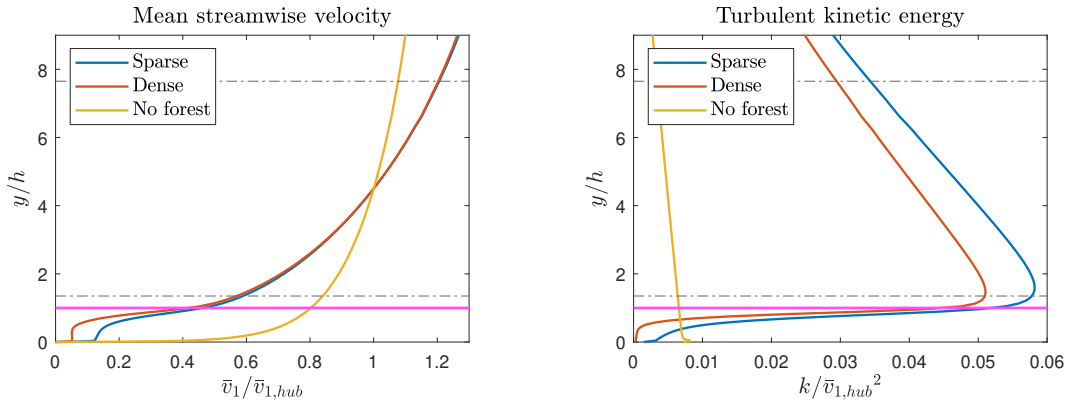

(a) The velocity profiles, the forest profiles are sheared as compared to no forest. No great difference can be seen between the sparse and dense profile within the rotor area.

(b) Turbulent kinetic energy for different forest profiles. The forest profiles seem exaggerated and displaced versions of the profile corresponding to 'No forest'.

Figure 4.6: Sanz's mean streamwise velocity profiles and TKE. The dashed and the magenta horizontal lines mark the rotor area $y \in [27 \text{ m}, 153 \text{ m}]$ and the tree line, respectively. The values are normalized with the tree height, h, and mean streamwise velocity, $\bar{v}_{1,hub}$.

Table 4.3: The ratio of mean streamwise velocity at hub height, $\bar{v}_{1,hub}$ and the reference wind speed $\bar{v}_{1,ref}$. Three fitted power exponents α are shown, each with a corresponding coefficient of determination R^2.

Forest profile	α	$\bar{v}_{1,hub}/\bar{v}_{1,ref}$	R^2
Sparse	0.3877	0.9472	0.9955
Dense	0.3950	0.9570	0.9917
No forest	0.1426	0.9955	0.9998

As displayed in Tab. 4.3 the mean streamwise velocities at hub height are lower for the sparse and dense forests compared with no forest. This is indicated by the ratio $\bar{v}_{1,hub}/\bar{v}_{1,ref}$: Given the same mass flow rate, $\bar{v}_{1,hub}$ is lower in forest regions. This is not apparent from viewing Fig. 4.6a due to the choice of normalization. Moreover, the negligible increase in the power exponent α for the dense forest, as compared to the sparse forest, indicates that both corresponding mean wind profiles are comparably sheared. Without a forest, the mean streamwise velocity within the rotor area is fitted almost perfectly (R^2 is close to 1) to the power exponent function. Furthermore, the

shear exponent for no forest region (α = 0.1426) is very much in line with a rule of thumb which states that over flat terrain, wind profiles have a power exponent $\alpha \approx 1/7$ [21].

Figure 4.6b displays the profiles for the turbulent kinetic energy, with differences clearly shown between forest types. With no forest, the position of the maximum TKE is close to the wall. In contrast, the position is above the canopies ($y/h \geq 1$) for the simulations with sparse and dense forests. Compared to no forest, the TKE is much greater almost everywhere in the vertical direction, except for a few meters above the wall. Interesting to note is that the sparse forest generates the most TKE overall. As previously discussed, it is likely that this result is not correct due to the limitations of Sanz's model. Moreover, the TKE gradients seem to increase due to the presence of a forest. However, as displayed in Fig. 4.2, accurately predicting the slopes of the TKE profiles above the forest canopies seem a shortcoming of the RANS canopy models. As observed earlier, the forest greatly shear the mean streamwise velocity profile, thus the velocity gradients are increased over the whole rotor area. This in turn increases the turbulent kinetic energy.

4.3 Wind turbine

In this section, the results for the wind turbine simulations are presented. This includes turbulent kinetic energy profiles, and a comparison of the power output for different forest densities. All results are based on simulations using Sanz's canopy model.

Figure 4.7 shows a comparison between the power curves for three different forest densities. The graph data is based on the steady-state wind with prescribed shear exponent (calculated by Sanz's model), simulated by FAST solver [23]. The curves show the power output of the wind turbine as a function of the wind velocity at hub height. The first data points appear at the cut-in speed, since lower velocities yield no power. For the sparse and dense forest, the curves are almost completely identical. With no forest, the power output is slightly lower for wind speeds between the cut-in speed and the rated speed. In all three cases, the power assumes a constant value of 5.3 MW for wind speeds higher than the rated speed. Clearly, the impact of the forest on the power is negligible.

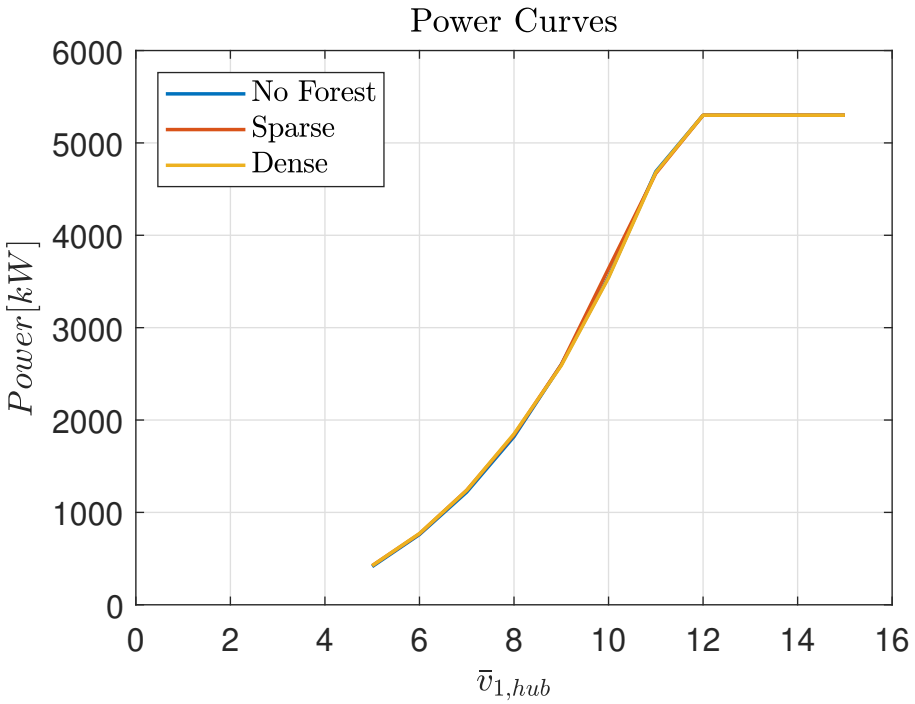

Figure 4.7: Comparison of the power curves for three forest settings: sparse, dense and no forest.

Figure 4.8 shows the turbulent kinetic energy profile for the case including the wind turbine actuator disc model, with forest, and the profile without the turbine for comparison. The reference velocity is $\bar{v}_{1,ref}$ = 8 m/s, and the forest is implemented using Sanz's model with the dense LAD profile. The TKE is plotted at a vertical line at the turbine's location, which is 300 m downstream from the inlet. With forest, the TKE is greater for almost the entire vertical range, as expected from previous results. The same is true when comparing the forest cases with and without the turbine. Adding the wind turbine causes a significant increase in the TKE, especially above the tree line and in the rotor area. The position of the maximum TKE is also higher for the wind turbine case, and is located at the lower edge of the rotor area.

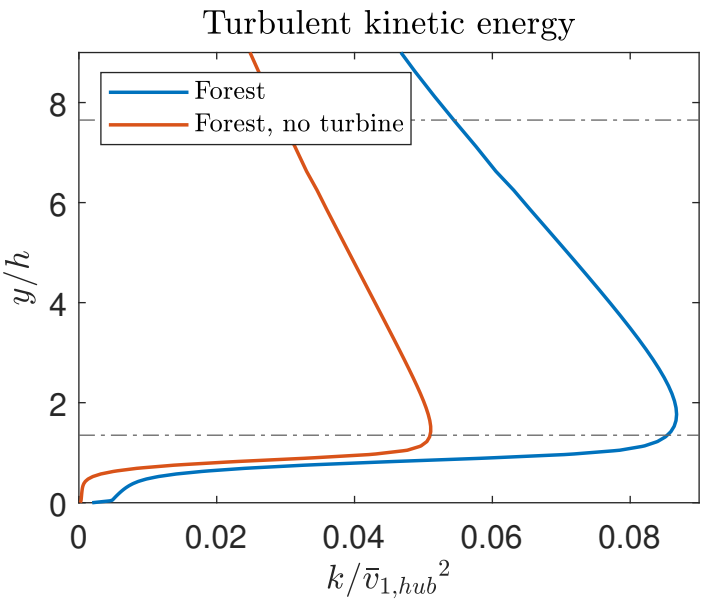

Figure 4.8: Turbulent kinetic energy for the wind turbine case, with dense forest using Sanz's model. TKE for dense forest without wind turbine added for reference. The horizontal dashed lines mark the rotor area.

4.4 Sources of error

As seen in Fig. 4.1a, at the very top the mean velocity gradients are zero for the canopy models, as opposed to the LES which is non-zero. However, all areas of interest have been below the top of the rotor area (y = 153 m). The symmetry condition is imposed high enough to leave results in this region largely unaffected by increases in domain height. This is supported by results of simulations conducted in a domain with a coarser mesh and 400 m in height. Curve fitting data from these simulations yields similar α for all canopy models, thus suggesting a domain height of 300 m is adequate.

The LES data is limited, with 64 points used for the rotor area. For the interval used, the end points correspond to y = 27.14 m and y = 153.78 m, such that the end points are chosen as the ones closest to the ends of the rotor area interval ($y \in [27$ m, 153 m$]$). Alternatively, only data strictly within the rotor area may be chosen, or the end points may be interpolated from the available data. Because of the limited amount of data, these decisions could impact the outcome. Depending on how the end points are chosen, it is observed that the curve fitted power exponent is in the range $\alpha \in [0.4151,$

0.4228]. The upper bound is almost high enough for Svensson's α to be closest to that of the LES. On a similar note, the data taken from STAR-CCM+ is linearly interpolated. However, it is hard to estimate its impact on the result.

Lastly, to determine which canopy model is best suited for the imposed conditions of this study, the method of comparing power exponents is only one of many. Alternatively, the mean streamwise velocities (normalized with $\bar{v}_{1,hub}$) of the canopy models could be compared by measuring their Root Mean Square Error (RMSE) with respect to the LES data. As seen in Tab. 4.4, such a comparison is in favour of Svensson's model for the sparse forest. Ultimately, all three canopy models predictions of $\bar{v}_1$ are good.

Table 4.4: The RMSE of the mean streamwise velocity for the three converged canopy models with respect to the LES data. The velocities are normalized with $\bar{v}_{1,hub}$. The RMSE values are calculated using same the data presented in section 4.1.1.

Canopy Model	RMSE
Sanz	0.0264
Green	0.0302
Svensson	0.0236

5

Conclusions

Conclusions that can be drawn from the first part of the project is that Sanz's model works the best in this study. Even though Sanz's worked that well is this study it might not be the case for other studies. However the use of the simulation performed in this study has its limitations. It is only possible to get a good result for flat regions with a homogeneous forest. To be able to use RANS as a reliable source for naturally occurring regions, many more simulations need to be performed. What is found by this study is that RANS can be used to get a preview of how wind farms will perform over a certain area. When new areas are investigated, simulations of similar forest regions must be used to verify the accuracy of the new simulation results. Having access to the real distribution of forest properties such as PAD covering the wind farm area (heterogeneous model) will increase the prediction accuracy level.

Another conclusion drawn is that the results for the dense forest simulations must be verified with LES performed for the dense forest. Because of the lack of LES for dense forest, the results for the dense forest are somewhat uncertain. When looking at Nebenführ's and Davidson's results [20], similarities can be observed and it is found that this strengthens the certainty of the results. Notable is that not the same type of forest and domain are used, which might impact the results. But with such similarities with both these LES and the sparse forest it is believed that the results for the dense forest are at least somewhat accurate.

Out of the tested canopy models that converged, all accurately described the mean streamwise velocity profiles. In contrast, they all struggled to capture the TKE near the forest height and Sanz's model was the most accurate out of the three. The presence of any forest also greatly increases the TKE when compared to bare ground. When comparing the difference between sparse and dense forest no major difference was seen in the mean streamwise velocity profiles. The TKE however seems to decrease with higher forest density for Sanz's model, but this is one of the drawbacks of using the

model. It underestimates the TKE which not supposed to happen. This is presented in section 4.1.4 and shown in the study by Nebenführ and Davidson [20] .

In other words, the TKE curve describing the dense forest is more similar to the curve for bare ground when using Sanz's model. It could be speculated that if the forest density tends to infinity, flow behaviour would be identical to bare ground as the forest height would behave like a solid wall boundary. What this thought experiment shows is that this project's forest parameters should give the TKE results observed with Sanz's model.

It can be seen that since any forest reduces the mean streamwise velocity at hub height there is a high velocity gradient near the forest height. The velocity gradient is also greater within the rotor area because of this when compared to no forest. This is seen in Fig. 4.6a as a curve closer to being horizontal throughout the rotor area. All turbulence is created from velocity gradients, this is also reflected in the results if the velocity profile is compared to the TKE profile. With a greater velocity gradient the TKE increases. This effect is most pronounced at the forest height, which makes the highest TKE present just slightly above this height.

Figure 4.7 shows that there is little observed difference in energy production when comparing different forest types with bare ground. This is because the bulk velocity is about the same. The turbulence is however increased which can be seen in Figs. 4.6b and 4.8. A higher turbulence in wind flow will fatigue a wind turbine faster than in wind flows with lower turbulence intensity. This means that turbines placed near forests can be expected to tr faster. This effect must be considered during planning and construction which increases cost. A higher cost for a given amount of power production might make investors look elsewhere.

Using periodic boundary conditions has some strengths and weaknesses. The drawback is that it cannot be used for the complex terrain and heterogeneous forest simulations. Important strengths are being cheaper to simulate as well as the capability to produce velocity profiles for use as inlet conditions in more expensive simulations.

Bibliography

[1] Bengtsson J. Sveriges klimatmål och klimatpolitiska ramverk;. Accessed: 31-01-2020. Available from: https://www.naturvardsverket.se/Miljoarbete-i-samhallet/Miljoarbete-i-Sverige/Uppdelat-efter-omrade/Klimat/Sveriges-klimatlag-och-klimatpolitiska-ramverk/.

[2] Holmström C. Elproduktion;. Accessed: 31-01-2020. Available from: https://www.ekonomifakta.se/fakta/energi/energibalans-i-sverige/elproduktion/.

[3] Spets Wojarski J. Sveriges och världens skogar;. Accessed: 31-01-2020. Available from: https://www.skogsindustrierna.se/skogsindustrin/branschstatistik/sveriges-och-varldens-skogar/.

[4] Flanker. Laminar boundary layer velocity profile;. Accessed: 14-04-2020. Available from: https://en.wikipedia.org/wiki/Boundary_layer#/media/File:Laminar_boundary_layer_scheme.svg.

[5] Jonkman J, Butterfield S, Musial W, Scott G. Definition of a 5-MW Reference Wind Turbine for Offshore System Development. National Renewable Energy Laboratory; 2009. Available from: https://www.nrel.gov/docs/fy09osti/38060.pdf.

[6] What is the Reynolds Number?;. Accessed: 05-05-2020. Available from: https://www.simscale.com/docs/content/simwiki/numerics/what-is-the-reynolds-number.html.

[7] Davidsson L. Fluid mechanics, turbulent flow and turbulence modeling. Göteborg, Sweden: Chalmers University of Technology; 2020.

[8] Versteeg HK, Malalasekera W. An Introduction to Computational Fluid Dynamics: The Finite Volume Method (2nd Edition). Pearson; 2007.

[9] Blazek J. Computational Fluid Dynamics: Principles and Applications. Oxford, United Kingdom: Elsevier Ltd; 2015.

[10] Simisiroglou N. Wind power wake modelling - Development and application of an actuator discmethod for industrial utilization. Department of Earth Sciences, Uppsala University,; 2018.

[11] Breakson K. CFD Modeling of a Neutral Atmospheric Boundary Layer over Complex Terrain; 2018. Available from: https://odr.chalmers.se/bitstream/20.500.12380/255128/1/255128.pdf.

[12] Lopes A, Laginha Palma J, Lopes J. Improving a Two-Equation Turbulence Model for Canopy Flows Using Large-Eddy Simulation. Boundary-Layer Meteorology. 2013 11;149.

[13] Bechmann A. Large-eddy simulation of atmospheric flow over complex terrain. Risø National Laboratory, Technical University of Denmark; 2007.

[14] Zhang X. CFD simulation of neutral ABL flows. Roskilde: Danmarks Tekniske Universitet, Risø Nationallaboratoriet for Bæredygtig Energi; 2009. 1688.

[15] Shaw R, Schumann U. E-ϵ Modelling of turbulent air flow downwind of a model forest edge. Boundary-Layer Meteorology. 1992;61:47–64.

[16] Katul GG, Mahrt L, Poggi D, Sanz C. One- and two-equation models for canopy turbulence. Boundary-Layer Meteorology. 2004 October;113:81–109.

[17] Liu J, Chen JM, Black MT, Novak MD. E-ϵ Modelling of turbulent air flow downwind of a model forest edge. Boundary-Layer Meteorology. 1996;77:21–44.

[18] Green SR. Large-eddy simulation of turbulent flow above and within a forest. University of British Columbia; 1995.

[19] Svensson U, Häggkvist K. A Two-equation turbulence model for canopy flows. Wind Engineering and Industrial Aerodynamics. 1990;35:201–211.

[20] Nebenführ B, Davidson L. Prediction of wind-turbine fatigue loads in forest regions based on turbulent LES inflow fields. Wind Energy. 2017;20(6):1003–1015. Available from: https://onlinelibrary.wiley.com/doi/abs/10.1002/we.2076.

[21] Wharton S, Lundquist J. Assessing atmospheric stability and its impacts on rotor-disk wind characteristics at an onshore wind farm. Wind Energy. 2012 05;15.

[22] Kelly M, Larsen G, Dimitrov NK, Natarajan A. Probabilistic Meteorological Characterization for Turbine Loads. Journal of Physics: Conference Series. 2014 jun;524.

[23] Jonkman J. FAST | NWTC Information Portal;. Accessed: 12-05-2020. Available from: https://nwtc.nrel.gov/FAST.

A

Figures

In section 4.1.2, a discussion is given for why the simulations using Liu's model did not converge. The residuals of those simulations are displayed in Fig. A.1. The residuals corresponding to 'x-momentum' have to be less than 10^{-4} in order for the stopping criteria to be fulfilled. As seen, this criteria is far from being met.

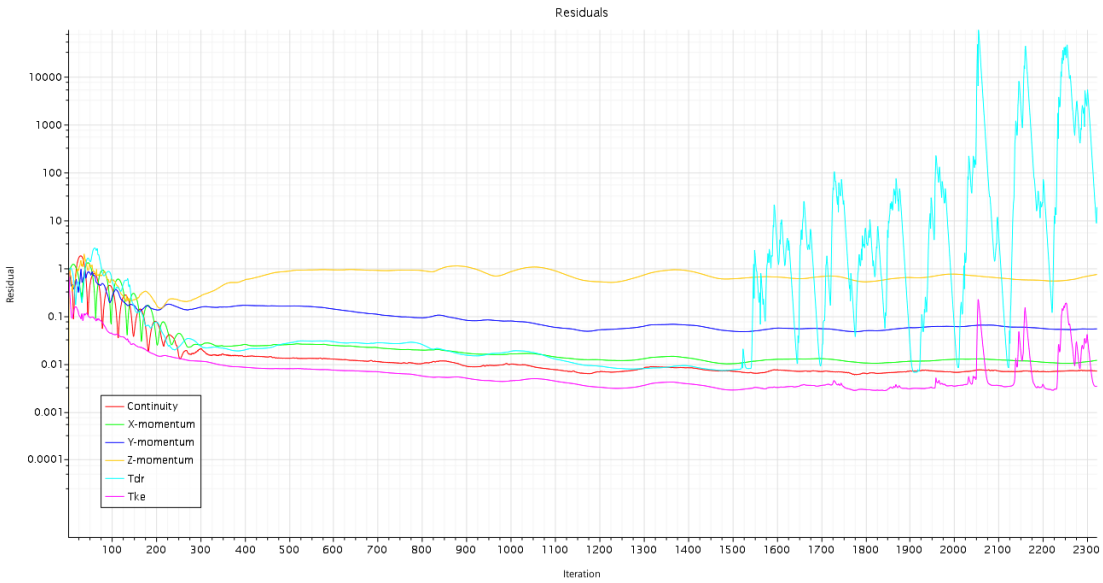

Figure A.1: Residuals for Liu's model. Non-converging. If a valid model is used all residuals should become small. Typically 10^{-4} or less.

In section 4.1.4 the mean streamwise velocity profiles for four different mass flow rates are shown side by side for the sparse forest. In contrast, Fig. A.2 features the velocity profiles for the dense forest. The same conclusion is drawn as from Fig. 4.3: Normalizing the velocity profiles yields nearly identical profiles regardless of mass flow rate.

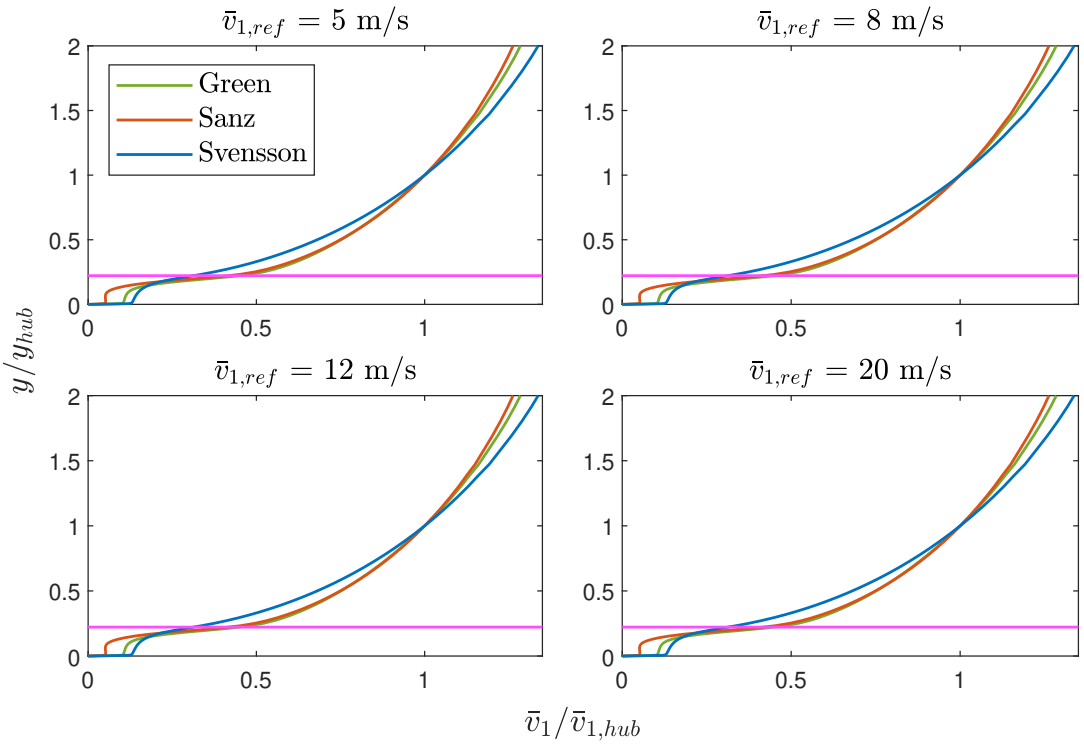

Figure A.2: Mean streamwise velocity profiles for the three converged canopy models. The results of four different simulated mass flow rates for the dense forest. When normalized, the velocity profiles are seemingly unaffected by the change in mass flow rate. The green horizontal lines represent the tree height.

B

Tables

In Tab. B.1 a full list of settings is given for the domain described in section 3.1.1.

Table B.1: Settings and properties for the (automated) mesh in STAR-CCM+.

Setting	Value
Base size	10 m
Number of prism layers	50
Prism Layer Near Wall Thickness	0.4 m
Prism Layer Total Thickness	125 m
Maximum Cell Size	10 m
Volume Growth Rate	Fast
Surface Growth Rate	1.3
Target Surface Size	10 m
Minimum Surface Size (% of base)	10 %
CAD Projection	Enabled
Maximum Core/Prism Transition Ratio	Disabled

In section 3.3 the performance data required by the actuator disc model is mentioned. This data is shown in full in table B.2, which includes the power, rotational speed and thrust coefficient as functions of the velocity at hub height.

Table B.2: NREL 5-MW turbine performance data. $\bar{v}_{1,hub}$ is the hub height velocity, Power is the rotor generated power, Rot. speed is the rotor angular velocity and C_t is the thrust coefficient.

$\bar{v}_{1,hub}$ [m/s]	Power [kW]	Rot. speed [rad/s]	C_t
5	470820	0.627	0.819
6	813570	0.753	0.819
7	1291920	0.878	0.819
8	1928460	1.003	0.819
9	2745790	1.129	0.819
10	3766520	1.255	0.819
11	4979230	1.2670	0.776
12	531590	1.2670	0.536
13	5312520	1.2670	0.397
14	530960	1.2670	0.309
15	5315740	1.2670	0.248
16	5306390	1.2670	0.203
17	5305110	1.2670	0.170
18	5312400	1.2670	0.144
19	5307740	1.2670	0.124
20	5306730	1.2670	0.107
21	5310170	1.2670	0.094
22	5317350	1.2670	0.083
23	5307830	1.2670	0.074
24	5319840	1.2670	0.066
25	5300170	1.2670	0.06

DEPARTMENT OF MECHANICS AND
MARITIME SCIENCES
CHALMERS UNIVERSITY OF TECHNOLOGY
GOTHENBURG, Sweden
www.chalmers.se

CHALMERS
UNIVERSITY OF TECHNOLOGY